Journal of Structural Geology 31 (2009) 523–539

Contents lists available at ScienceDirect

Journal of Structural Geology

journal homepage: www.elsevier.com/locate/jsg

Formation of orogen-perpendicular thrusts due to mechanical contrasts in the basal décollement in the Central External Sierras (Southern Pyrenees, Spain)

Oskar Vidal-Royo [a,*], Hemin A. Koyi [b], Josep Anton Muñoz [a]

[a] Geomodels Institute, GGAC, Departament de Geodinàmica i Geofísica, Facultat de Geologia, Universitat de Barcelona, C/ Martí i Franquès s/n, 08028 Barcelona, Spain
[b] Hans Ramberg Tectonic Laboratory, Department of Earth Sciences, Uppsala University, Villavägen 16, SE-752 36 Uppsala, Sweden

ARTICLE INFO

Article history:
Received 24 November 2008
Received in revised form
19 February 2009
Accepted 17 March 2009
Available online 27 March 2009

Keywords:
Analogue modelling
External Sierras
Southern Pyrenees
Pico del Aguila
Detachment
Ductile deformation
Brittle deformation

ABSTRACT

Two series of analogue models are used to explore the effect of ductile-frictional contrasts of the basal décollement on the development of oblique and transverse structures during thin-skinned shortening. These models simulate the evolution of the Central External Sierras (CES; Southern Pyrenees, Spain), which constitute the frontal emerging part of the southernmost Pyrenean thrust. The CES are characterised by the presence of N–S to NW–SE anticlines, perpendicular to the Pyrenean structural trend and developed in the hanging-wall of the thrust system. They detach on unevenly distributed Triassic materials (evaporitic–dolomitic interfingering). The models simulated the effect of adjacent ductile versus frictional décollements during shortening. Model Series A tests the thickness ratio between overburden and the ductile layer, whereas model Series B tests the width (perpendicular to the shortening direction) of frictional décollement. Model results confirms that deformation reaches further in areas detached on a ductile layer whereas above frictional décollement areas, shortening is accommodated by additional uplift and penetrative strain. This replicates the structural style of the CES: higher structural relief of N–S anticlines with regard to orogen-parallel structures, absence of a representative ductile décollement in the core, plunging towards the hinterland and foreland-side closure not thrusted by the South Pyrenean thrust.

1. Introduction

The evolution and final geometry of a fold-and-thrust belt is strongly dependant on the mechanical properties of the basal detachment level (Davis and Engelder, 1985; Cotton and Koyi, 2000; Costa and Vendeville, 2002; Bahroudi and Koyi, 2003; Koyi and Cotton, 2004; Massoli et al., 2006). Scaled analogue models have been widely used to simulate the kinematics of thrust-and-fold belts detached on brittle substrates (Mulugeta and Koyi, 1987; Mulugeta, 1988; Mulugeta and Koyi, 1992; Liu et al., 1992; Koyi, 1995, 1997; Storti et al., 2001; Koyi and Vendeville, 2003; Lohrmann et al., 2003; McClay et al., 2004; McClay and Whitehouse, 2004) and less often on viscous ductile substrates (Letouzey et al., 1995; Cotton and Koyi, 2000; Costa and Vendeville, 2002; Grelaud et al., 2002; Schreurs et al., 2002; Smit et al., 2003; Dooley et al., 2007; Crespo-Blanc, 2008). The dynamic evolution and the final geometry of fold and thrust belts depend on the mechanical behaviour of the basal décollement and its interaction with the overlying overburden (Davis and Engelder, 1985; Koyi, 1988; Cobbold et al., 1989; Talbot, 1992; Harrison, 1995; Cotton and Koyi, 2000; Costa and Vendeville, 2002; Grelaud et al., 2002; Schreurs et al., 2002; Bahroudi and Koyi, 2003; Luján et al., 2003; Bonini, 2007; Storti et al., 2007).

The geometry and structural style of the Pyrenees depend on the interaction between the intracrustal inhomogeneities inherited from the pre-collisional Early Cretaceous extensional event and the weak horizons in the cover sequence, mostly Triassic and Eocene salts, shales and evaporites (Beaumont et al., 2000). The external domains of the southern Pyrenees commonly show a highly irregular and hard to predict distribution of the detachment level (widely believed to be Triassic evaporitic facies; e.g. Keuper or middle Muschelkalk), often with scarce and variable thickness of allochtonous transported detachment materials at the frontal emerging thrust areas (Pocoví, 1979; Muñoz, 1992; Millán, 1995; Teixell and García-Sansegundo, 1995; Oliva et al., 1996; Teixell and Koyi, 2003; Oliva-Urcía and Pueyo, 2007). These external domains (e.g. Serres Marginals and External Sierras) correspond to pieces of the South-Pyrenean foreland basin that were incorporated into the orogen as deformation progressed southwards. Paleogeographic reconstructions indicate that in late Triassic, the region was located

* Corresponding author. Geomodels Institute, GGAC, Departament de Geodinàmica i Geofísica, Facultat de Geologia, Universitat de Barcelona, C/ Martí i Franquès s/n, 2nd floor, office 227, 08028 Barcelona, Spain. Tel.: +34 934 035 957; fax: +34 934 021 340.
E-mail addresses: oskarvidal@ub.edu, vidal.oskar@gmail.com (O. Vidal-Royo).

0191-8141/$ – see front matter © 2009 Elsevier Ltd. All rights reserved.
doi:10.1016/j.jsg.2009.03.011

in a structural high of the Triassic extensional basin (see Fig. 10.12 of López-Gómez et al., 2002; Castillo-Herrador, 1974; Jurado, 1990; Salvany, 1990). Consequently, in the External Sierras just a thin sequence of Upper Triassic sediments was deposited.

Many modelling studies have focused on the structure of the Pyrenean external domains and provided new insights on their evolution (Nalpas et al., 1999; Soto et al., 2002, 2006; Teixell and Koyi, 2003; Koyi and Sans, 2006; Storti et al., 2007). Our study focuses on the central sector of the External Sierras (CES; Southern Pyrenees, Spain), where the main structural pattern is characterised by the interference between E–W orogen-parallel structures and a set of N–S kilometric-scale, thrust-related anticlines.

Different hypothesis have been suggested to explain the geodynamic evolution of the Central External Sierras. Based on the irregular fold geometries, the ubiquitous evaporitic strata along the décollement and in the core of the fold cores, the timing of folding and palinspastic restorations of the folds and Jaca basin, it has been suggested that the N–S anticlines could be a consequence of the halotectonic deformation related to the extensional faults affecting the older part of the stratigraphic sequence (Anastasio, 1992; Anastasio and Holl, 2001) or rotation of the thrust sheets (Pueyo et al., 2002). Pueyo et al. (2002), used paleomagnetic data to report a 40° clockwise rotation of the South-Pyrenean thrust sheets.

Based on field evidence of inhomogeneous distribution of Upper Triassic gypsum-bearing clays, this paper explores the mechanical contrasts in the basal décollement and the consequent differential propagation of the deformation in the overburden to explain the generation of oblique and transverse N–S anticlines during a single N–S shortening phase in the CES. Marques and Cobbold (2002, 2006) have also tackled the differential propagation of deformation in compressional regimes, in which the thickness variation resulted in differential topographic formation and differential propagation. However, the aim of this work is to give new insights on the geodynamic evolution of the central sector of the External Sierras by carrying out series of analogue models that explore the differential propagation of deformation as a direct response of mechanical changes in the basal detachment.

2. Geological setting

The External Sierras constitute the frontal emerging part of the southernmost Pyrenean thrust sheets (Soler and Puigdefàbregas, 1970; IGME, 1992; Millán et al., 1994; Millán, 1995; Pueyo et al., 2002). The External Sierras consist of a system of thin-skinned imbricated thrust sheets detached on clayish, dolomitic and evaporitic Middle and Late Triassic facies (Keuper and Muschelkalk facies). The hanging-wall of the frontal Pyrenean thrust involves an Upper Triassic to Lower Miocene sedimentary sequence (Puigdefàbregas, 1975; Millán et al., 1994; Millán, 1995) which was displaced southwards over the Tertiary sediments of the Ebro foreland basin. The External Sierras also constitute the southern limit of the Jaca piggy-back basin, which was incorporated into the Pyrenean orogen during the last stages of deformation, since Middle Eocene times (Millán, 1995).

One of the peculiarities of External Sierras is the presence of a set of irregularly spaced transverse NW–SE to N–S anticlines. These structures are at high angle or perpendicular to the general structural trend of the Pyrenees (E–W; tectonic transport towards the south) and create a complex interference structural pattern (Fig. 1). These N–S anticlines become younger and smaller westwards (Millán et al., 1994; Millán, 1995) and their growth was synchronous with the deposition of the Middle Eocene to Oligocene sediments and the development of the South-Pyrenean thrust front (which was active until Early Miocene; Puigdefàbregas, 1975; Holl and Anastasio, 1993; Millán et al., 1994; Millán, 1995). From an accurate observation of the growth strata pattern, Poblet et al. (1997) considered N–S folds to form by partially limb lengthening, limb rotation and flexural slip mechanisms, under high

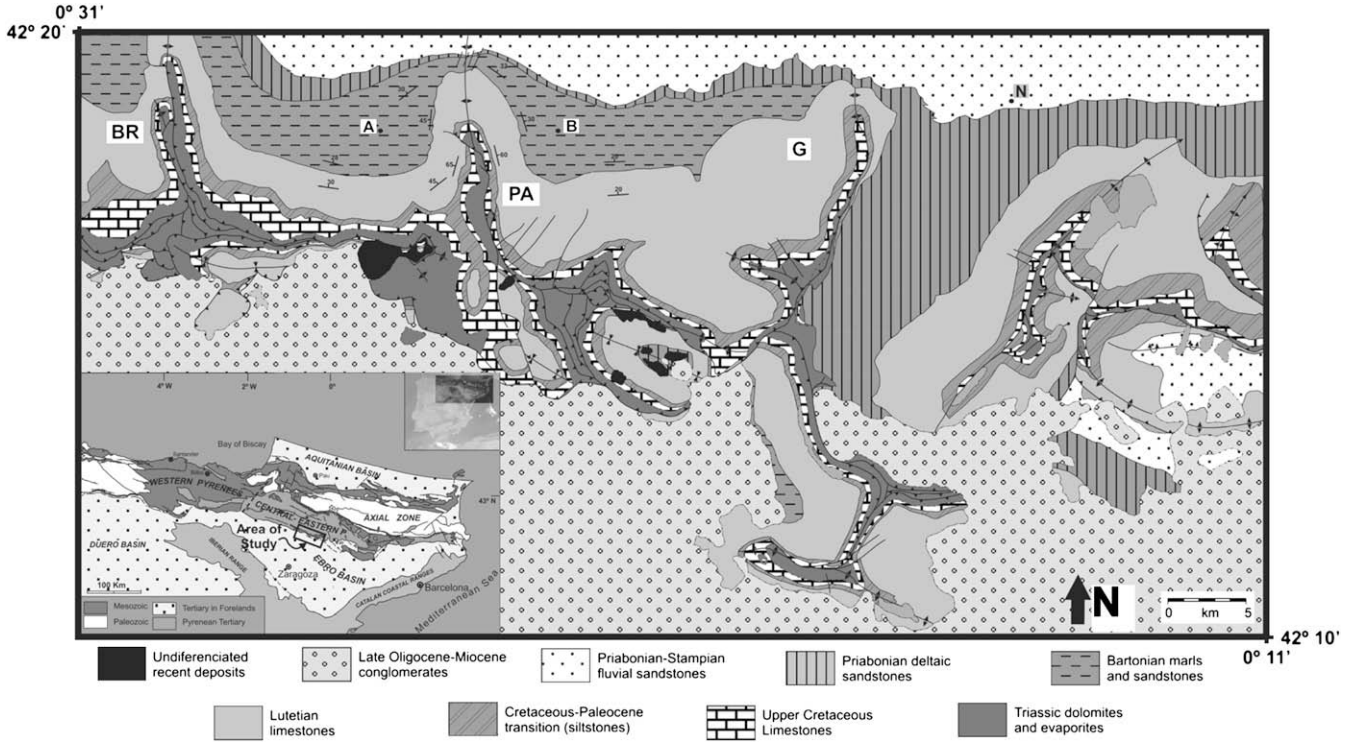

Fig. 1. Geological map of Central External Sierras (modified after IGME, 1992). BR: Bentué de Rasal anticline; PA: Pico del Águila anticline; G: Gabardiella anticline complex; A: Arguis Village; B: Belsué Village; N: Nozito Village.

sedimentation rates. Given that the size of the N–S anticlines decreases westwards, it can be assumed that the deformation also diminished in the same direction (i.e. the amount of shortening decreased westwards). Since the present study especially focuses on the processes that took place in the N–S anticlines of the central sector of the Sierras (Fig. 1), the general descriptions will mainly refer to this area, and not necessarily to the rest of the External Sierras.

The stratigraphy in the study area consists of a relatively thin (few hundred metres thick) Mesozoic succession, covered by a thicker Paleogene sequence (Fig. 2). The Mesozoic is made of Triassic limestones, dolomites and gypsum-bearing clays, and Upper Cretaceous shallow marine limestones. The Paleogene comprises continental sandstones, siltstones and lacustrine limestones of the Cretaceous–Paleocene transition (Garumnian facies), shallow marine platform limestones of the Guara Formation (Lutetian), shallow marine and transitional marls, limestones and sandstones of the Arguis and Belsué–Atarés Formations (Upper Lutetian to Middle Priabonian), and the fluvial clays, sandstones and conglomerates of the Campodarbe Formation (Middle Priabonian to Middle Oligocene).

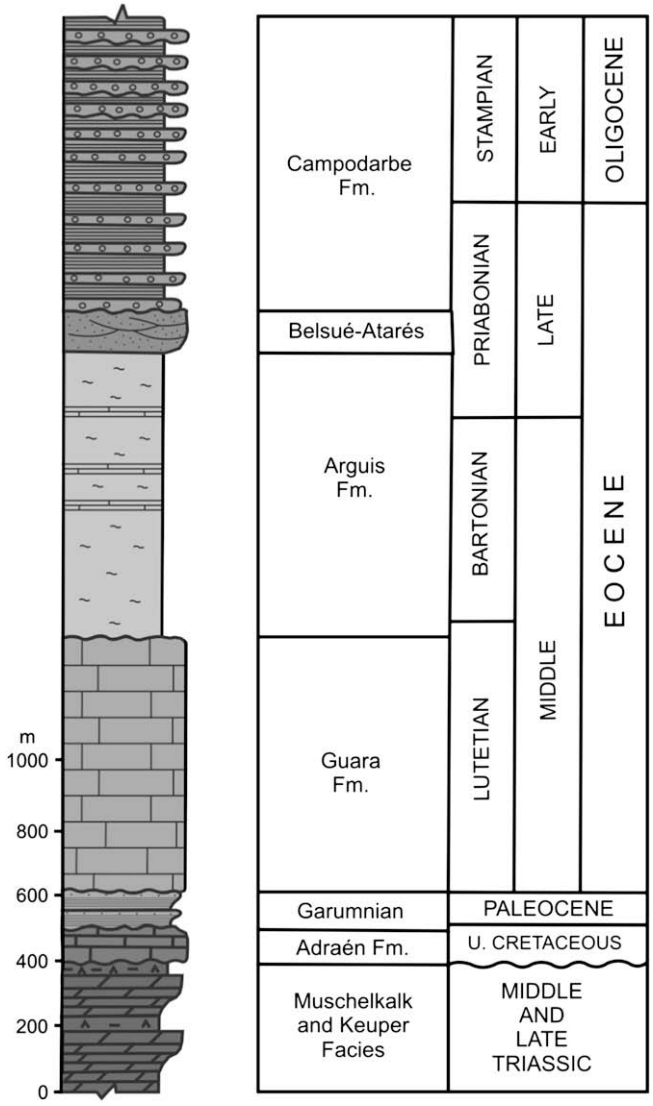

Fig. 2. Stratigraphic sequence described in Central External Sierras (modified after Millán et al., 1994). Note that the stratigraphic thickness of Guara Fm. may vary across the region.

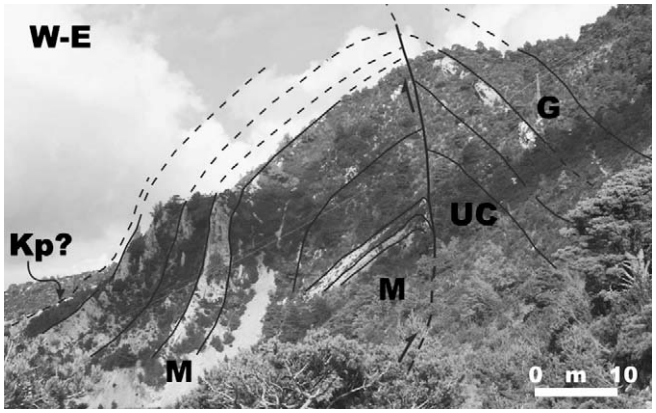

Fig. 3. Sketch of the core of Pico del Águila anticline. The internal folded thrust affects the core of the structure placing Muschelkalk Middle Triassic rocks (M) on Upper Cretaceous (UC) and Garumnian (G) rocks. Keuper evaporitic facies (Kp) can not be recognised and just a thin sequence may outcrop at the left of the picture.

The first attempts to determine the geodynamic evolution of the External Sierras were given by Mallada (1878), Selzer (1948) and Almela and Ríos (1951), who proposed a progressive westward migration of the deformation. Anastasio (1992) and Anastasio and Holl (2001) proposed a halokinetic origin of the N–S trending folds of the External Sierras. According to those studies, the N–S structures developed as a result of the differential loading caused by the progradation of Paleogene clastic distributary systems. This differential loading resulted in the flow of the Triassic mobile décollement towards the west, where the overburden units are thinner. Flow of Triassic evaporites in front of the wedge resulted in the formation of a trough that accommodated additional loading. However, this argument does not seem to hold for the study area because according to Poblet and Hardy (1995), the thickness of the overburden is 4.3–1.6 times the thickness of the ductile unit. Moreover, the overburden/substrate thickness ratio was possibly higher if we take into account the fact that Triassic sediments

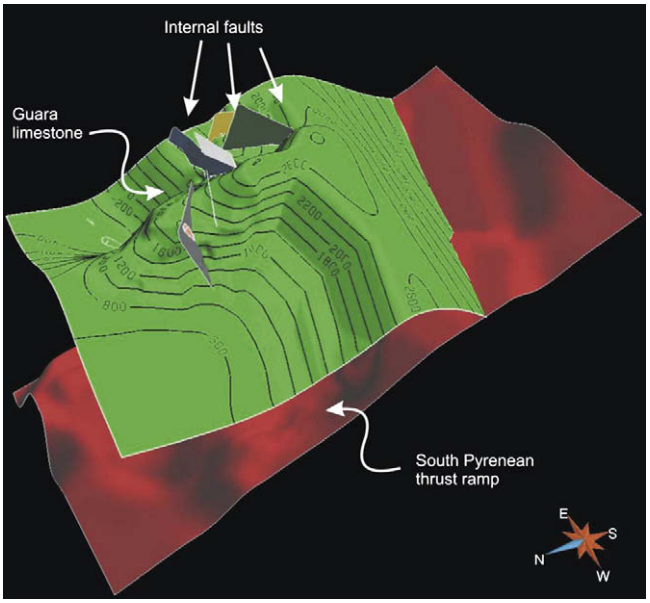

Fig. 4. 3D reconstruction of the Pico del Águila anticline (top of Guara Fm. in green) and the ramp of the frontal South-Pyrenean emergent thrust (in red). Notice both northern and southern closures of the anticline. Guara Fm. describes an orogen-parallel E–W structural trend in the accommodation area of the thrust.

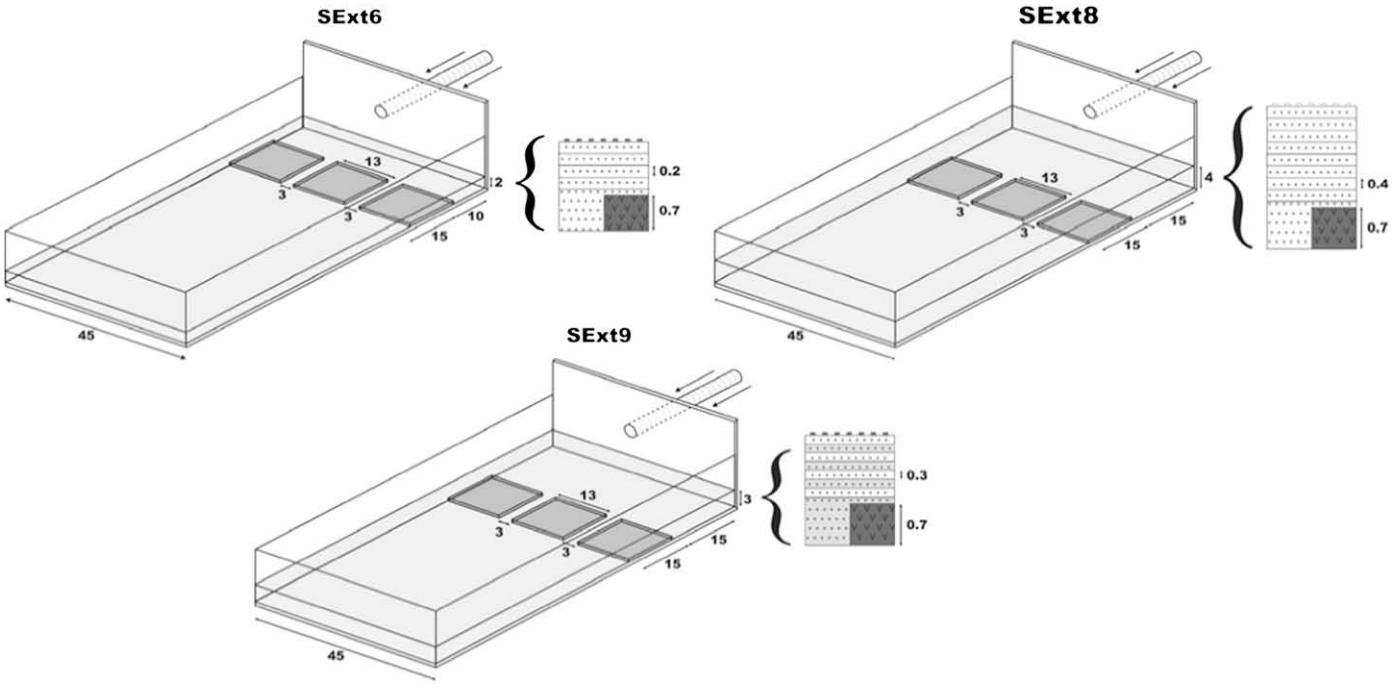

Fig. 5. Initial setup of model series A showing the distribution of ductile (SGM-36) and brittle (sand) décollements and direction of shortening. The stratigraphic sequence of each model is also presented. All the values are in cm.

predominantly consist of competent lithologies such as Muschelkalk limestones and dolomites, and Keuper evaporites and gypsum-bearing clays are nearly absent. These facts led us to decline the halokinetic origin of N–S anticlines proposed by Anastasio (1992) and Anastasio and Holl (2001).

Later, based on a meticulous mapping and stratigraphic analysis of the synfolding sequence (Millán et al., 1994) as well as several paleomagnetic studies (Pueyo, 2000; Pueyo et al., 2002, 2003a), a new evolutionary model was proposed, which we outline below. During the early stages of the evolution of the External Sierras (Early Lutetian to Chattian), the thrust system was characterised by a south-verging main thrust and a set of arcuate north–eastward concave, oblique thrusts. The N–S trending folds are interpreted as a more evolved stage of the initially oblique thrusts, which were generated as detachment folds on a hanging-wall flat over footwall flat thrust configuration. In addition to a general translation towards the south, a regional clockwise rotation process characterised the kinematics of the thrust system (up to 40° measured at the base of Arguis Fm, western limb of Pico del Águila anticline; Pueyo et al., 2002). Clockwise rotation has played an important role on the kinematics of the Sierras, as it is reported in many studies (e.g., Dinarés et al., 1992; Bentham and Burbank, 1996; Hogan and Burbank, 1996; Pueyo et al., 1997, 2000, 2002, 2003a,b; Pueyo, 2000; Larrasoaña et al., 2001; Oliva et al., 1996; Oliva-Urcía and Pueyo, 2007). However, during Chattian to Early Miocene, the structural evolution changed abruptly. The rotating thrust system was folded and truncated by the formation of the Santo Domingo detachment anticline and its associated south-directed thrust system, located in the western sector of the External Sierras (beyond the western limits of Fig. 1). Consequently, the remaining N–S trending folds occurred at the hanging-wall of the new Santo Domingo thrust system, representing the northernmost portion of those oblique structures (the rest of the structures are supposed to be either buried under the continental deposits of the Ebro foreland basin or

Table 1
Scaling parameters between models and nature.

Parameter	Nature	Models	Scaling ratio
Acceleration due to gravity	9.81	9.81	$a_m/a_n = 1$
Thickness (m)			
Overburden	~750–1000	0.013–0.033	$l_m/l_n = 10^{-5}$
Substrate	~300	0.007	$l_m/l_n = 10^{-5}$
Mean density ρ (kg/m^3)			
Overburden	2550	1700	$\rho_m/\rho_n = 0.67$
Substrate	2200[a]–2550[b]	987[a]–1700[b]	$\rho_m/\rho_n = 0.45$–0.67
Density contrast $\Delta\rho$ (ρo–ρs)	350[a]–0[b]	713[a]–0[b]	$\Delta\rho_m/\Delta\rho_n = 2.04$–?
Friction coefficient of overburden	0.85	0.73	0.86
Viscosity of ductile layer (Pa · s)	$10^{-18\ (\text{to}\ -19)}$[c]	5×10^4	$10^{-14\ (\text{to}\ -15)}$
(ρl g/τ_0) ratio	0.75	0.16	0.21
Shortening rate	0.35–0.99 mm/year[d]	16.2×10^4 mm/year	46.3×10^4–16.2×10^4

Subscripts m, n, o, s denote, respectively, model, nature, overburden and substrate.
[a] Ductile substrate.
[b] Frictional substrate.
[c] Estimated value.
[d] Extracted from Poblet and Hardy (1995).

isolated by erosion under the southern limb of the Santo Domingo anticline, according to (Pueyo et al., 2002). The emplacement of these N–S trending folds in a hanging-wall flat over footwall ramp position of the Santo Domingo thrust system is the cause to their 30° plunge towards the North (Millán, 1995; Pueyo et al., 2002).

Although this is the best reported and data-based hypothesis about the evolution of the Central External Sierras, it presents some weak points that have led us to look for other complementary processes. Previous studies have stated that the N–S trending Pico del Águila fold detach on Upper Triassic rocks (Pueyo et al., 2002). Nonetheless, both field observations and geological mapping (IGME, 1992) indicate that Muschelkalk limestones and dolomites (Middle Triassic rocks) are the oldest materials outcropping in the core of the anticline (Fig. 3) and are internally thrusted, showing high internal deformation. On the other hand, although Keuper clays and evaporites (Upper Triassic rocks) outline the geometry of the fold as the rest of the upper Mesozoic sequence do, important decrease of thickness is observed towards the inner part, where it is nearly absent in the core of the anticline (Fig. 3). In such a way, Keuper facies are thicker and better exposed in the areas between, rather than in the core of the N–S anticlines, where the frontal South-Pyrenean thrust emerges.

From the reported 40° clockwise rotation it can be inferred that the initial oblique structures had to form at least at 50° relative to the shortening direction. This is a decisive fact in the present orientation of these transverse structures. However, there is no explanation for the mechanism of generation of those arcuate, oblique structures formed in Early Lutetian to Chattian times. In addition, the 3D geometrical reconstruction of the N–S trending

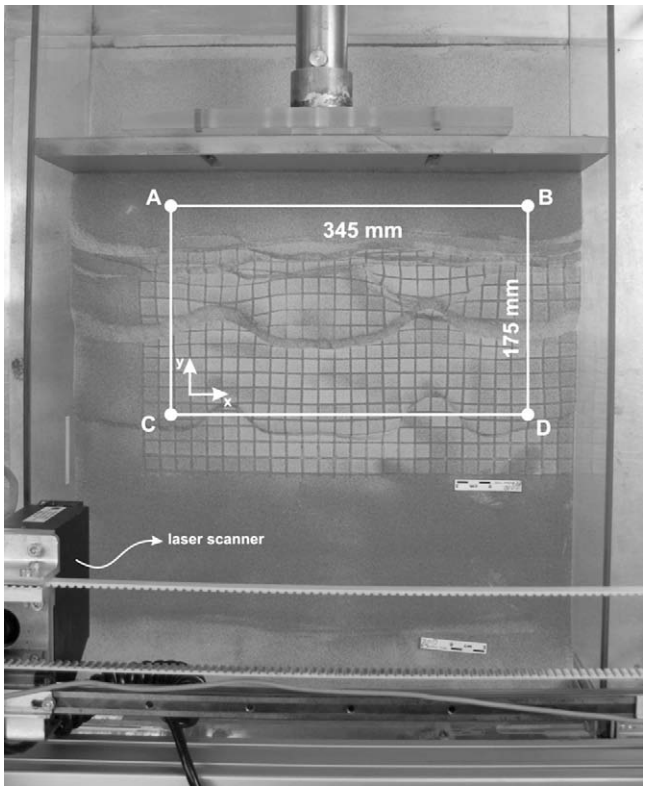

Fig. 6. Top view of model SExt10 after 20% shortening. Laser scanner is visible at the left bottom of the picture. ABCD indicate the dimensions of the scanned area in the last stage of deformation. The area covers only the central portion of the model, avoiding wall perturbations of the laser beam. AB distance was kept constant for all the scans, whereas AC distance was decreased as shortening increased. C and D positions were constant. A and B positions were progressively closer to the fix wall.

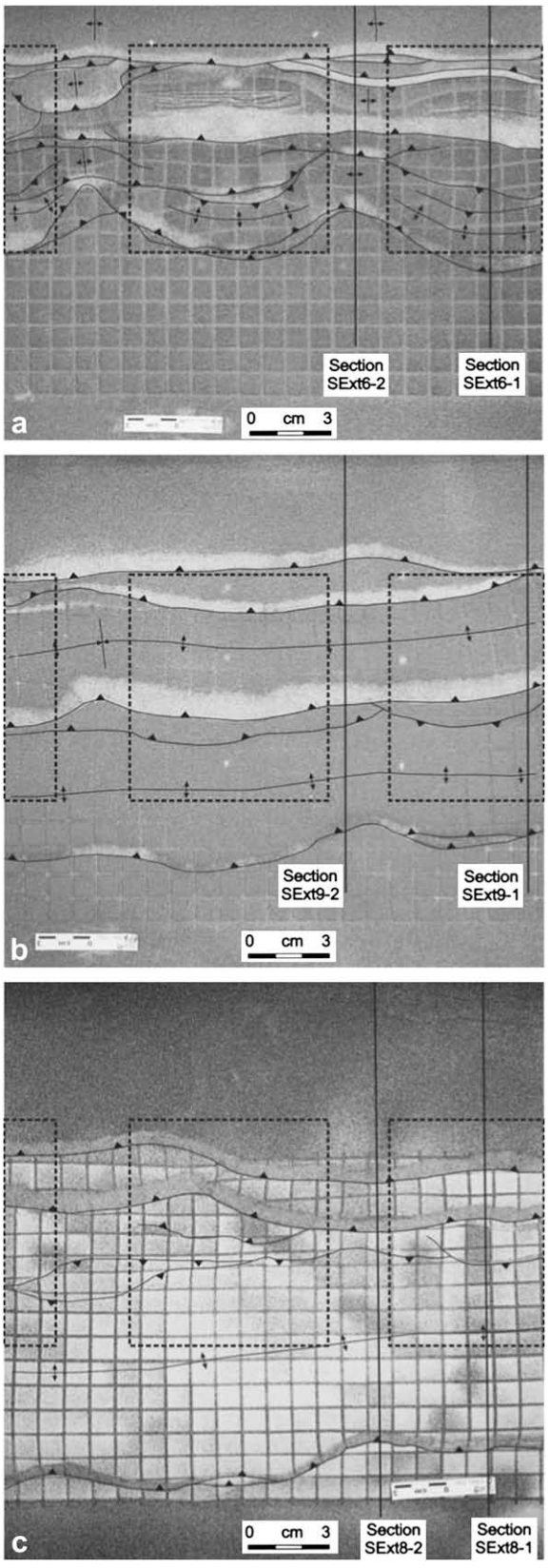

Fig. 7. Top view of models SExt6 (a), SExt9 (b) and SExt8 (c) after 20% of shortening. Representative sections of the models are indicated on the top view and showed in Fig. 8 for SExt6, Fig. 9 for SExt9 and Fig. 10 for SExt8. Dashed rectangles indicate the initial position of the ductile layers in the basal décollement. Notice the clear differential propagation of deformation and the generation of transverse structures in model SExt6 (a) and the general orogen-parallel style of models SExt8 (b) and SExt9 (c).

Pico del Águila anticline (Fig. 4) indicates that this structure was not truncated by the Santo Domingo thrust system. As shown, both northern and southern closures of Pico del Águila are observable northwards of the South-Pyrenean thrust. The southern closure of Pico del Águila shows a slight plunge towards the south (around 10°), and the bedding of Guara Formation shows an orogen-parallel E–W attitude along the thrust front. Therefore, there are no evidences of structural interference in the South-Pyrenean frontal emergent thrust supporting the truncation of the initially arcuate oblique structures by the emplacement of the Santo Domingo thrust system.

3. Model series

3.1. Modelling procedure and materials

Two series of experiments were executed for this study. The experimental design is based on field observations indicating a nearly absence of Keuper facies in the core of the transverse anticlines (e.g. Pico del Águila and Gabardiella anticlines, Fig. 1), and a thicker presence of these materials where the orogen-parallel structures develop (e.g. South-Pyrenean thrust front). All the models consisted of a colour interlayered sequence of sand covering an uneven basal level where three ductile silicone patches were present (Fig. 5). Dry quartz sand with a density of 1700 kg m^{-3}, cohesive strength C of 140 Pa and sieved to an average grain size of 35 μm was used to simulate the brittle sedimentary cover of Upper Cretaceous to Lutetian rocks. The Triassic irregular detachment level was simulated by means of the Newtonian viscous silicone putty SGM36 (density of 987 kg m^{-3} and effective viscosity η of 5×10^4 Pa s at room temperature, manufactured by Dow Corning Ltd.) neighbouring dry quartz sand (Fig. 5). A summary of the scaling parameters used in this study is shown in Table 1. For detailed analysis of these materials and their suitability as model analogues, see Weijermars (1986) and Weijermars and Schmeling (1986). All the experiments were built at the Hans Ramberg Tectonic Laboratory, in a deformation rig with a basal aluminium plate on which sand was glued to give a high friction. All models had a fixed width of 45 cm, an initial length parallel to the compression piston of 60 cm, a constant detachment thickness of 7 mm (for both silicone and sand), and were shortened at a constant rate of 1.85 cm h^{-1} ($5.14\ 10^{-6}$ m s^{-1}) up to 20% during 6 h. A passive grid of square markers (12×12 mm) was printed on the top surface of the models, which was photographed during shortening at regular intervals in order to record the evolution of the model at surface. After 20% of shortening, the deformed models were covered by loose sand and impregnated by water, which increased the cohesive strength of sand and allowed sectioning of the model.

In one of the Series B models (model SExt10) we used a high-accuracy laser scanner (±0.1 mm; Nilforoushan et al., 2008) to monitor the topographic evolution of the model. Technical descriptions of this device and discussions about its use and benefits can be found in Williams et al. (2000), Swantesson (2005),

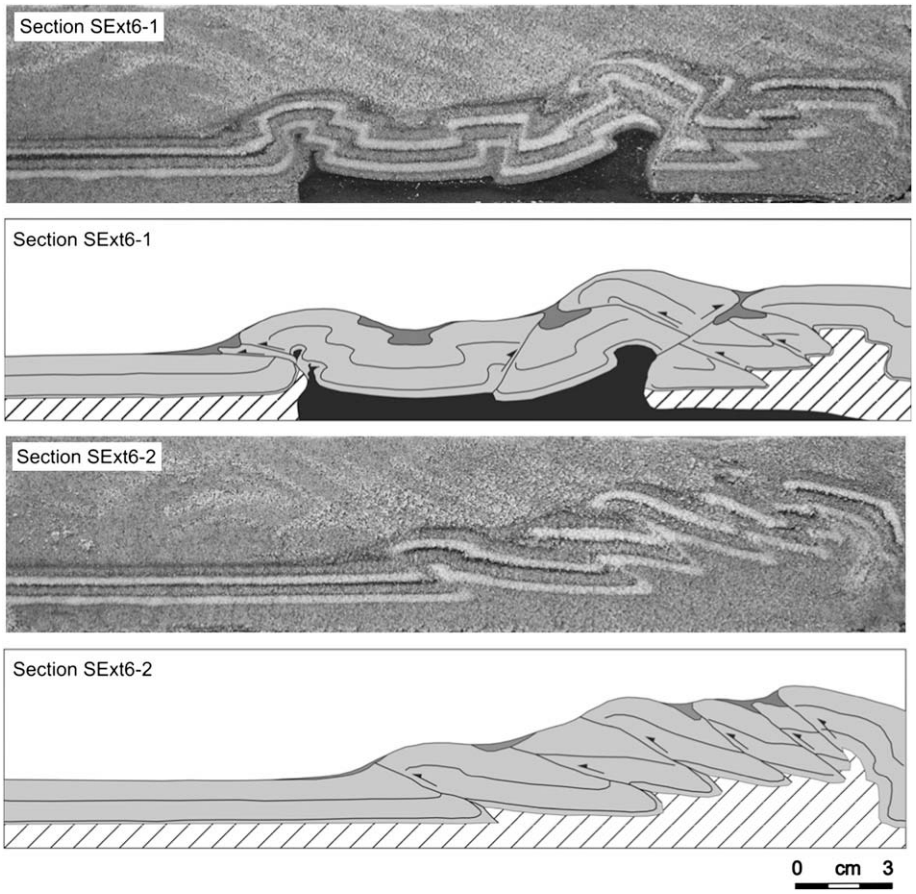

Fig. 8. Pictures and line-drawings of two representative cross-sections of model SExt6 (see Fig. 7a for location) showing the low friction domain (Section SExt6-1) and the high friction domain (Section SExt6-2). Black area represents the ductile layer (SGM-36) and dashed line areas represent the frictional décollement (pure loose sand). Notice how deformation front reaches further in SExt6-1 than in SExt6-2. In contrast, SExt6-2 shows a slightly additional uplift compared to SExt6-1. The structural pattern is also different: interference of fore-thrusts and back-thrusts in SExt6-1, and an imbricate foreland verging stack in SExt6-2.

Swantesson et al. (2006) and Nilforoushan et al. (2008). By using a laser scanner, lateral and vertical movements of the model surface were monitored during shortening. In such a way, model SExt10 was scanned at every 3–4% of bulk shortening, monitoring the differential advance of the deformation front and the surface topography. To avoid edge effects on the laser beam only the central portion of the model was scanned (Fig. 6).

3.2. Modelling strategy

Our intention by gluing sand onto the basal plate was to force high friction behaviour in the basement in order to accentuate the contrast between the ductile décollement (silicon layers) and the frictional décollement (sand). The aim of this irregularly distributed detachment level was to test how lateral contrasts in friction were able to cause the generation of arcuate, oblique and even transverse structures regardless of the orientation of the shortening.

The series of experiments aimed to test different parameters that have demonstrated to be decisive in the formation of shortening-parallel structures. In Series A, we explored the ratio between cover and detachment thicknesses as a parameter to control the generation of wavy structures. In Series B, the width of the high friction detachment areas was changed.

3.3. Limitations of the models

We have not investigated the effect of mechanical properties of the cover units; increasing competence of cover units is expected to have a similar effect as increasing the thickness of the cover units. In addition, the role of strain rate and its influence on the brittle-ductile coupling have not been investigated in our modelling, although this could be an important factor able to influence model deformation. Folds developed above very weak décollements (i.e., with low viscosity and deformed at low strain rates) are expected to become comparatively more amplified (and localise more deformation) than in case of stronger décollements (Bonini, 2003). From this point of view, one may thus speculate that, by producing more amplified folds, weak décollements may reduce the variations in topographic altitudes between HF and LF compartments, whereas strong décollements would tend to amplify such differences. In this work, the effect of syntectonic sedimentation was not studied either.

Finally, these models have been designed with a regular distribution of the detachment materials: three rectangular ductile layers separated by two rectangular sand layers. Although this regularity is necessary to understand the role of each parameter investigated, the distribution of the detachment materials in nature must be more complicated and irregular, creating a wide variety of particular structures and styles.

4. Model kinematics and results

Shortening of the models caused deformation in both the sand and the silicone layers. The deformation pattern was different between areas detached on the high frictional level and those detached on the ductile level. The results presented hereby are

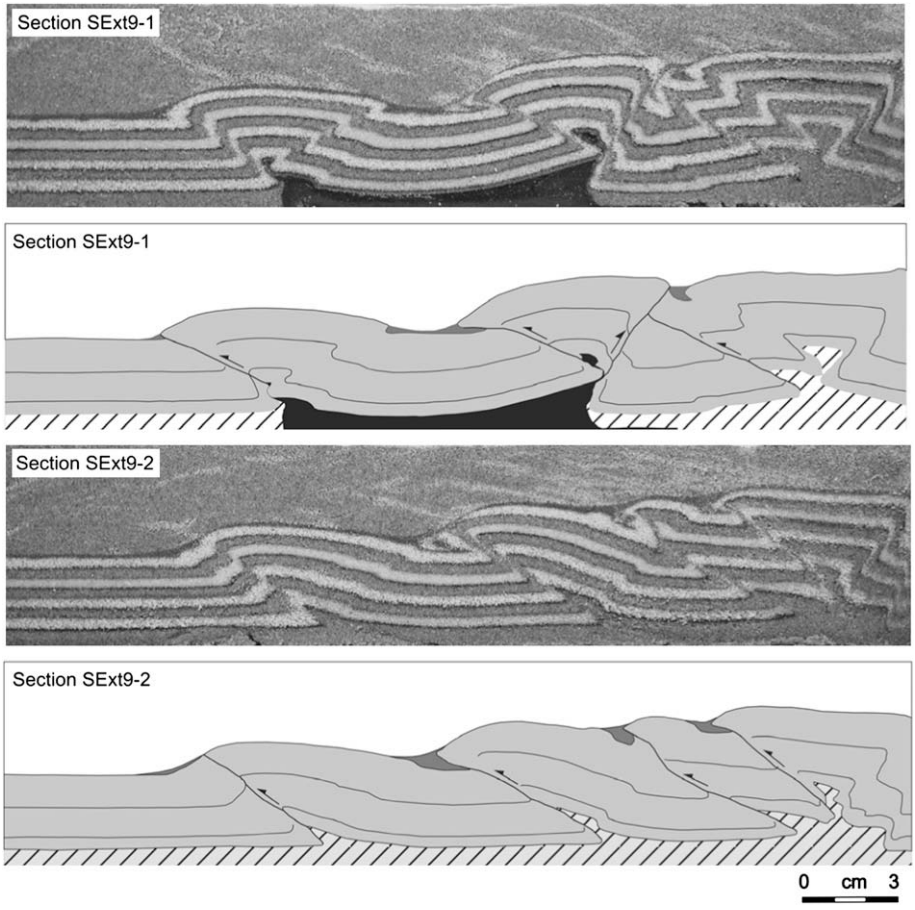

Fig. 9. Pictures and line-drawings of two representative cross-sections of model SExt9 (see Fig. 7b for location) showing the low friction domain (Section SExt9-1) and the high friction domain (Section SExt9-2). Symbols and abbreviations are as those in Fig. 8. Although no steep changes were found in top view between the frictional and the ductile domain, the structural pattern is noticeably different in both sections: interference of forward and backward thrusts in SExt9-1, and an imbricate foreland verging stack in SExt9-2.

shown by following an order according to the explored parameter. In such a way, the resulting experiments are classified in Series A and Series B since they are evaluating cover/detachment thickness ratio and distance between ductile layers (i.e. width of high friction areas), respectively.

4.1. Model Series A

Three experiments have been conducted to evaluate the role of the thickness ratio between the cover and the detachment. To do so, a constant detachment thickness of 0.7 cm was kept in different models, whereas cover thickness was changed (Fig. 5): 2 cm in model SExt6, 3 cm in model SExt9, and 4 cm in model SExt8. Transverse structures have been obtained only in model SExt6, while the other two models showed only slightly wavy structures (SExt9) or even a general straight structural style (SExt8) (Fig. 7). Despite this, both models SExt6 and SExt9 show a steep contrast in structural style between areas detached on ductile layers and areas detached on sand (Cotton and Koyi, 2000). The areas detached on frictional décollement (high friction areas = HF areas) are characterised by a forward directed imbricate stack developed by a piggyback thrusting sequence (Cotton and Koyi, 2000; Costa and Vendeville, 2002; Luján et al., 2003) (Figs. 8 and 9). On the other hand, areas detached on ductile décollement (low friction areas = LF areas) are characterised by the development of both forward and backward thrusts. Nevertheless, model SExt8 shows a homogeneous straight structural pattern that does not change across the model, regardless of the basal detachment changes. In this model, the structural style is characterised by a set of foreland verging, widely-spaced thrusts (Fig. 10). In this particular case, the forward edge of the silicon patches (pinch-out) has acted as a buttress to nucleate the development of the frontal thrust all across the model.

The transverse anticlines generate above the high friction areas where the hanging-wall shows the least advance, accommodating the deformation by uplift in comparison to the neighbouring LF areas, where deformation front advances further forwards. Topographic evolution above the LF and HF areas differs significantly (Fig. 11). Reference points located above the high friction décollement reach a higher altitude than the points located above the ductile décollements. In model SExt6, this differential topographic uplift occurs after 15% shortening, whereas in model SExt9 it occurs after 13% shortening. Despite this, the contrast in uplift between high friction and ductile areas is clearly less in model SExt9. In model SExt6, the altitude increases by 9% above the frictional décollement relative to the ductile décollement. In models SExt8 and SExt9, the difference in elevation is around 6%. In models SExt6 and SExt9, deformation front above LF areas reached further than above HF areas. However, thickness of the cover units influences this differential propagation, which is larger in model SExt6, where cover units are thinner, than in SExt9, where cover units are thicker (Figs. 7a,b). However, in model SExt8, propagation of the deformation front above the frictional and ductile décollements is entirely different compared to the other two models (models SExt6 and SExt9). At early stages of shortening, the advance of the deformation front and the increase of the altitude follow a progressive, continuous, sub-parallel path in HF and LF areas, with

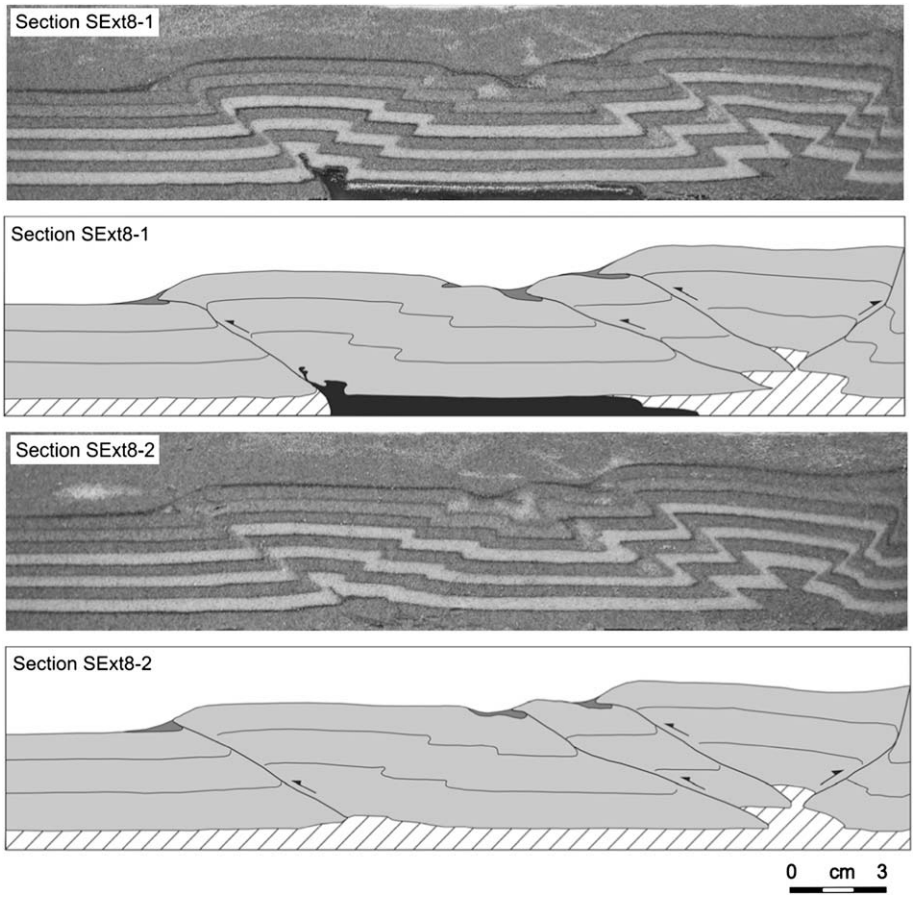

Fig. 10. Pictures and line-drawings of two representative cross-sections of model SExt8 (see Fig. 7c for location) showing the low friction (Section SExt8-1) and the high friction domains (Section SExt8-2). Symbols and abbreviations are as those in Fig. 8. Since the overburden unit is thicker than in other models (3.3 cm), the structural style does not change across the model, which is characterised by predominant foreland verging thrusts with associated smaller backward structures developed in the back limbs.

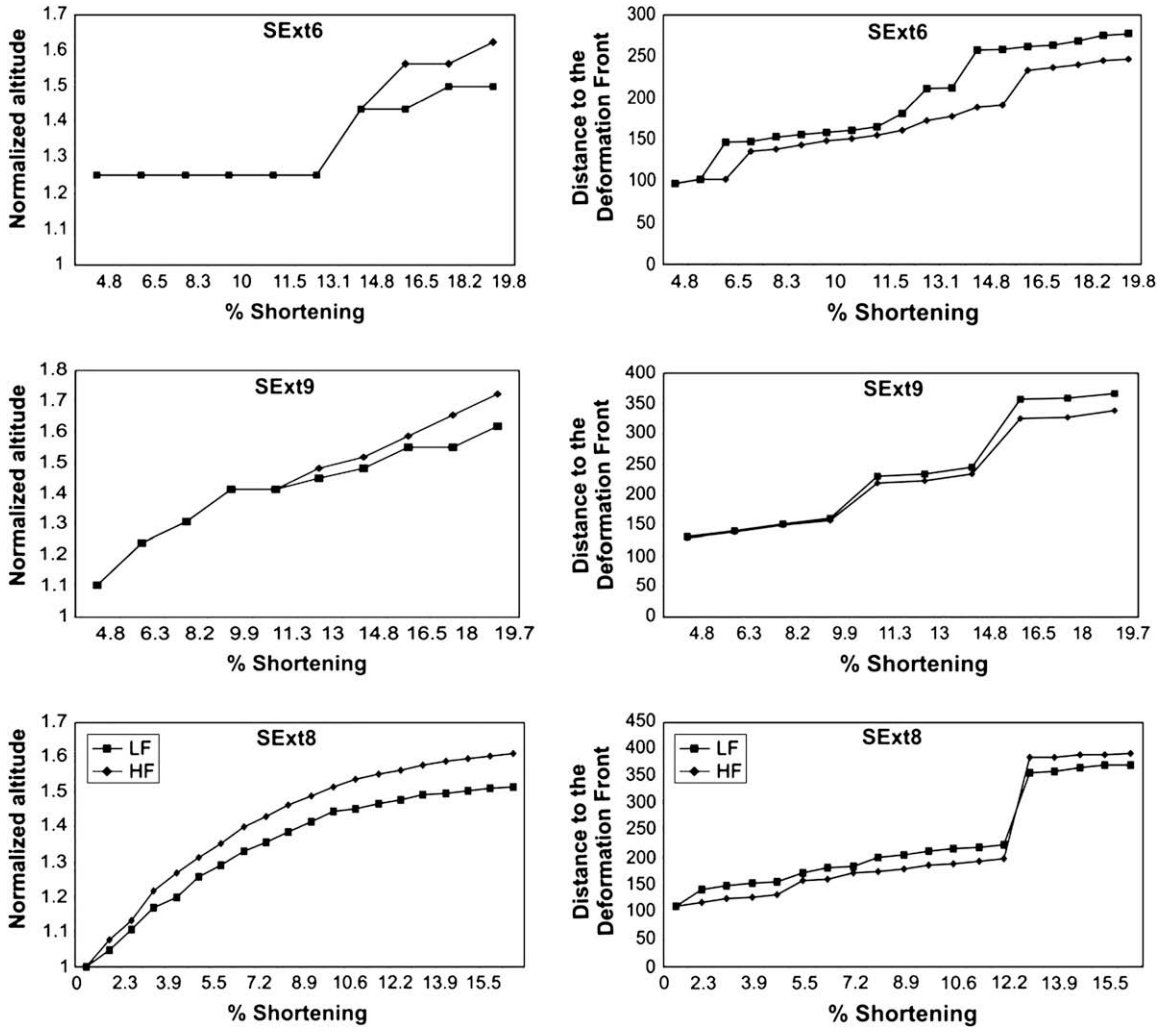

Fig. 11. For each experiment, left plots show the variation of the normalised altitude of the model at two control points plotted against percentage of shortening, whereas right plots show distance to deformation front plotted against percentage of shortening. Control points were placed on the surface of the model; one on HF areas and one on LF areas, before shortening to track the displacement/altitude variation. These plots show the evolution of the different domains of each model. SExt6 and SExt9 show the expected response of the overburden to an irregularly distributed décollement: higher advance of LF areas and higher uplift of HF areas. However, SExt8 shows a larger uplift and a larger advance of HF areas. Consequently, SExt8 behaviour is considered to be independent of the detachment distribution due to the larger thickness of the overburden.

LF areas reaching slightly further than HF ones. Nevertheless, after 12.2% of shortening, the last frontal thrust is created, and causes a slight extra advance of HF areas with respect to LF areas. However, this shift is considered to be negligible and the frontal thrust is interpreted as a nearly straight structure, formed regardless the mechanical contrasts in the basal décollement.

4.2. Model Series B

The width of HF areas has been explored in this series of experiments to test its effect on the generation of oblique/transverse structures. For a given stratigraphic thickness, two different HF widths have been considered. Model SExt9, described previously, had a HF area width of 3 cm and a LF area width of 13 cm, whereas model SExt10 had a HF area width of 6 cm (twice as that in model SExt9) and a LF area width of 11 cm (Fig. 12). During shortening, transverse structures formed only in model SExt10, while model SExt9 showed just slightly wavy structures at the deformation front. As model SExt9 has been described earlier, descriptions will mainly refer to model SExt10, whose top-view was monitored with a high-resolution scanner.

Using the data from the laser-scanner, topographic evolution of the model in 3D was monitored (Fig. 13) and topographic profiles were generated which were compared between different areas of the model (Fig. 14).

Deformation in model SExt10 started with formation of three straight forward directed thrusts, formed in the rear part of the model in a piggy-back style after 6% bulk shortening (Fig. 13b). After 9% bulk shortening, deformation reached the ductile layers, when a clear differential advance of the deformation front was noticed between areas detached on the ductile layers and areas detached on sand; deformation front propagated further above the DD (Figs. 13c and 14). With further shortening, model top view shows that deformation front above HF areas does not advance as far as it does above LF areas (Fig. 15). This creates a structural pattern constituted by wavy thrusts (along strike) that transport further the areas detached on a ductile layer than the areas detached on sand (Cotton and Koyi, 2000; Bahroudi and Koyi, 2003). As a consequence, areas detached on sand accommodate the deformation by an additional uplift with regard to areas detached on a ductile layer, developing gentle transverse anticlines in the hanging-wall of the thrusts (Figs. 14C–C′). After 16% of bulk shortening, existing structures are not

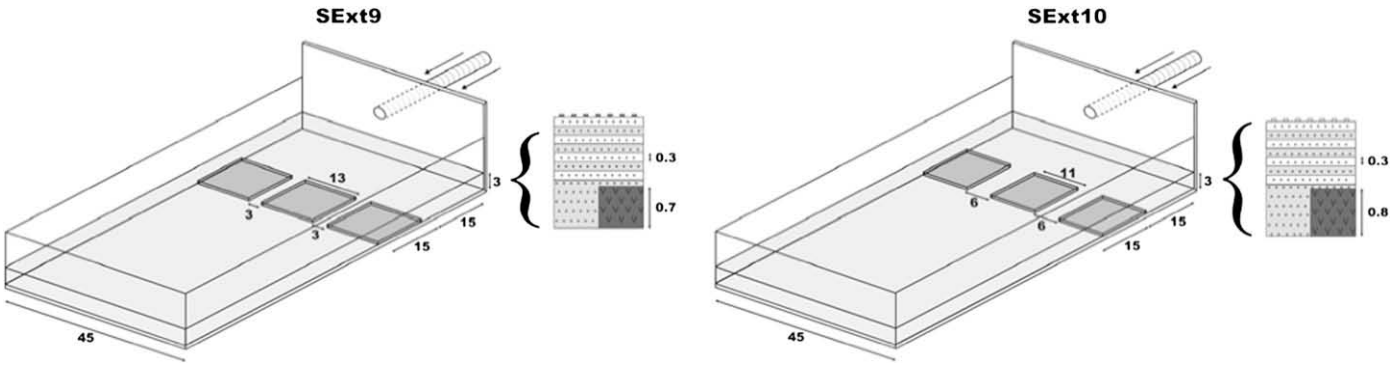

Fig. 12. Initial setup of model Series B showing the distribution of ductile (SGM-36) and brittle (sand) décollements and the shortening orientation. The stratigraphic sequence of each model is presented aside. All the values are in cm.

able to accommodate more deformation and new structures form causing the deformation front to migrate towards the foreland (Fig. 13e). At this stage, a second generation of transverse structures is formed in continuation with the previous ones. After 20% bulk shortening (Figs. 13f and 15), the geometry of the deformation front is similar to that observed in the previous generation of transverse structures (formed after 9% bulk shortening). Nevertheless, the location of the thrust front in the LF areas coincides with the frontal pinch-out of the basal ductile layers (Fig. 16). This indicates that the last generation of structures has been forced to form above the pinch-out of the ductile layers, as a consequence of the mechanical contrast between silicone and sand.

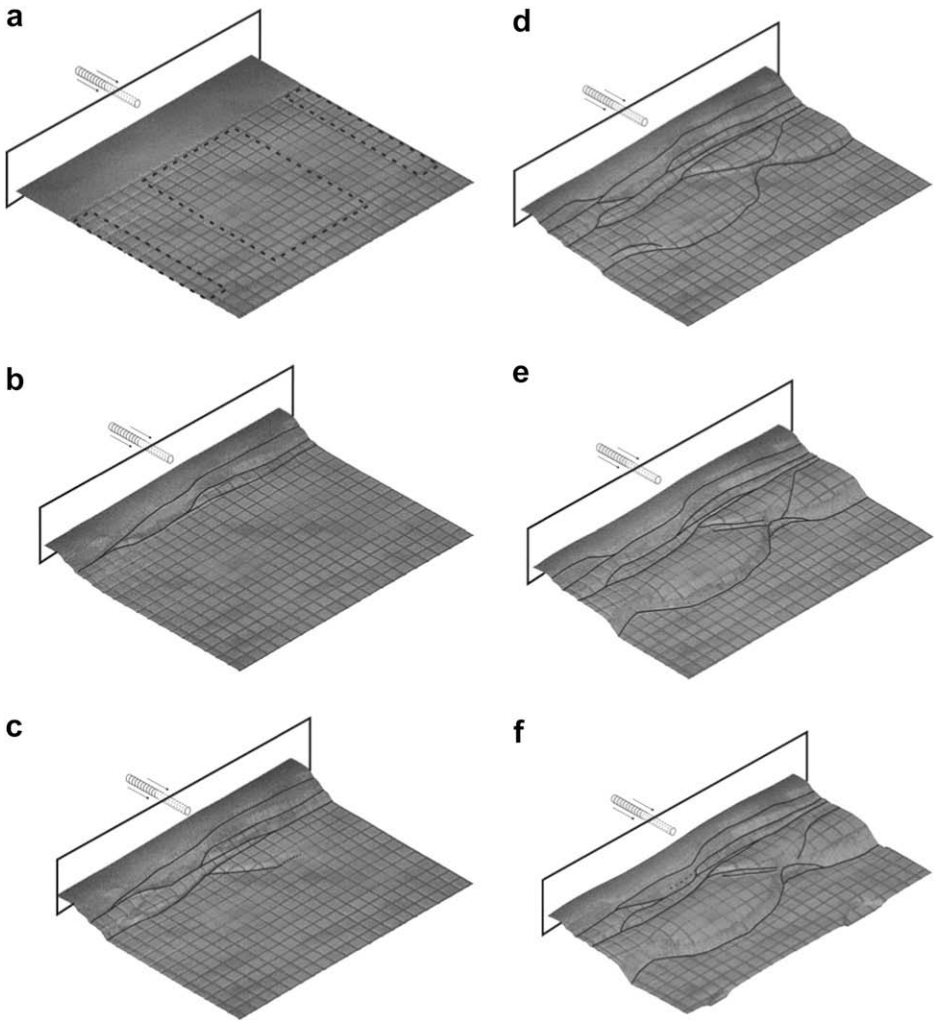

Fig. 13. 3D views of the model topography generated from laser scan data with the main thrusts mapped onto it, at different stages of deformation: (a) initial setup (dashed rectangles indicate the initial position of the ductile layers in the basal décollement); (b) 3% of shortening; (c) 6% of shortening; (d) 10% of shortening; (e) 16% of shortening; and (f) and 20% of shortening. This allows controlling the three-dimensional variation of topography depending on which type of décollement is located beneath.

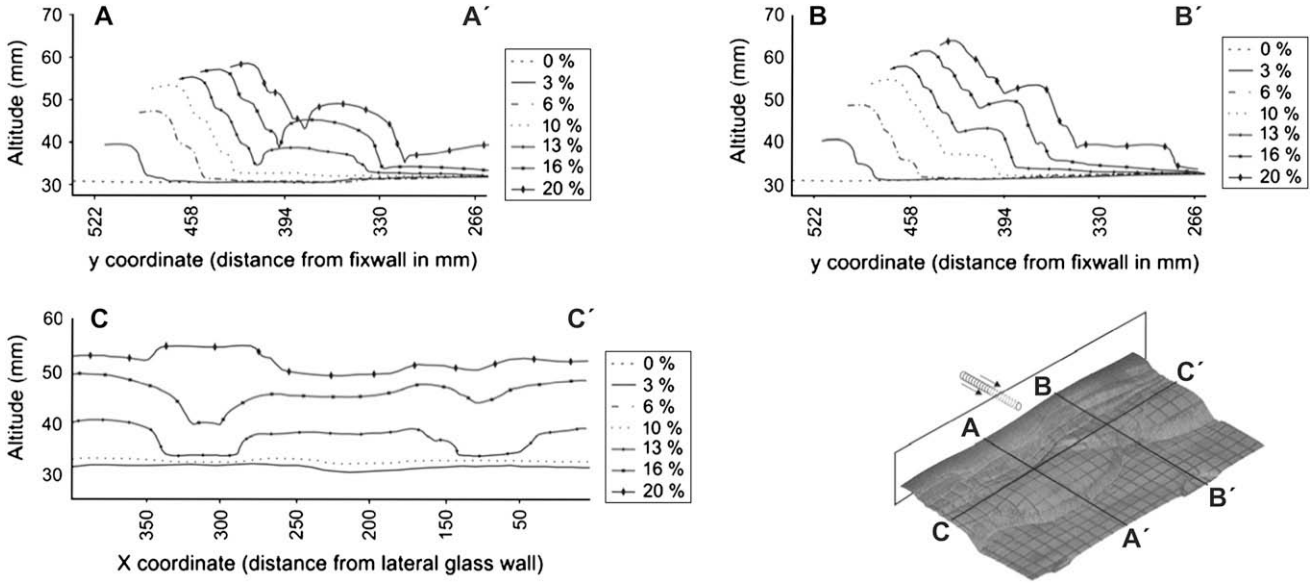

Fig. 14. Topographic variation of the models along three profiles. Vertical scale exaggerated. A–A′: profile located along LF décollement. B–B′: profile located along HF décollement. C–C′: profile located across the model, involving both LF and HF décollements. Comparison of A–A′ and B–B′ points out the different evolution of the cover along the different décollements. C–C′ profile shows how HF areas were initially depressed since deformation front arrives later than in LF areas (curves at 0%, 3% and 6% are overlapped since deformation front reaches C–C′ after 6% bulk shortening). In other words, LF areas were firstly but less uplifted. However, when deformation front reaches the profile location at the HF domain, it becomes uplifted since higher friction causes a different accommodation of shortening.

For model SExt10, three different types of sections have been taken: (1) vertical sections parallel to the shortening direction; (2) vertical sections perpendicular to the shortening direction; and (3) horizontal sections (Figs. 16 and 17). The structural style along shortening direction is similar to the one reported for model SExt6 (Fig. 16). A set of foreland verging thrusts and some associated minor back-thrusts are the common features. In sections perpendicular to shortening direction, higher uplift of HF with regard to LF areas (Figs. 17a,b) is observed. The horizontal section shows depth variation in the structural style and the change in the differential propagation of the thrusts with depth (Fig. 17c). In general, horizontal sections show the internal geometry of the layers with depth as well as the relation between orogen-parallel structures and the oblique/transverse ones.

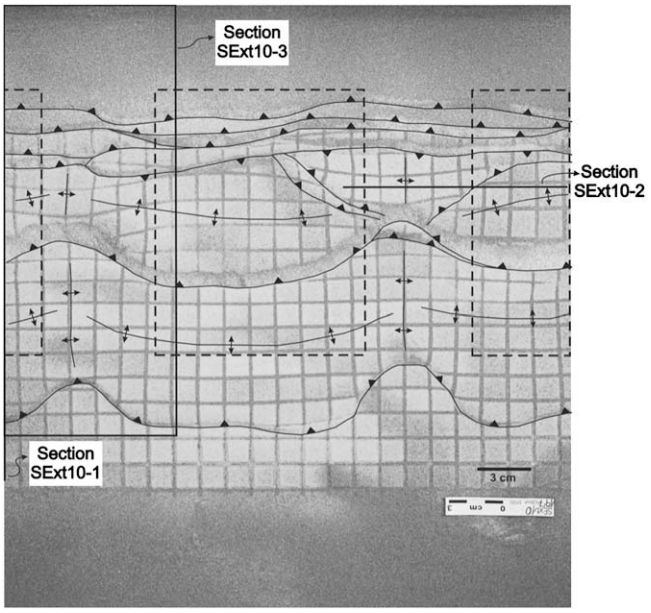

Fig. 15. Top view of the model SExt10 after 20% of shortening. Three types of sections have been taken for this model: parallel-to-shortening (Section SExt10-1, Fig. 16), perpendicular-to shortening (Section SExt10-2, Figs. 17a,b) and horizontal sections (Section SExt10-3; Fig. 17c). Dashed rectangles indicate the initial position of the ductile layers in the basal décollement. As in model SExt6, both orogen-parallel structures (LF areas) and transverse structures (HF areas) have been obtained in the hanging-wall of the thrusts.

Development of oblique and transverse structures shown in model SExt10 is a consequence of the mechanical contrast between HF and LF areas. In such a way, the deformation of ductile layers by flow, ductile thickening and folding is laterally transferred to HF areas, where lateral thrust ramps climb up section from the ductile layers at their lateral pinch-outs. These lateral ramps merge in the core of the HF areas, uplifting and gently deforming the units above, and highly faulting the units below (Figs. 17a,b). This results in a lateral migration of ductile layers towards HF areas and the thickening along the HF/LF boundary where the lateral ramps detach (Figs. 17a,b). In horizontal sections, where the internal geometry of the layers is shown at depth, the layers show general foreland verging thrusts in which lower units are thrusted and upper units are gently folded. Only a periclinal closure is observed in the orogen-side of the transverse structures (Fig. 17c). This indicates that these structures slightly plunge towards the orogen ought to the tilting created by the emplacement of the frontal foreland verging thrust.

5. Discussion

The main aim of this work is to understand the oblique and transverse structures in the Central External Sierras. Here, a new idea is proposed based on the influence of the irregularity of the detachment level without invoking either longitudinal E–W contraction or significant rotations along a vertical axis (which would only accommodate only maximum 40° of clockwise rotation of the structure; Pueyo et al., 2002).

The intention of this paper is naturally not to "replace" the hypothesis of the vertical axis rotation in External Sierras, which is documented in the field. The aim of this study is to give a viable

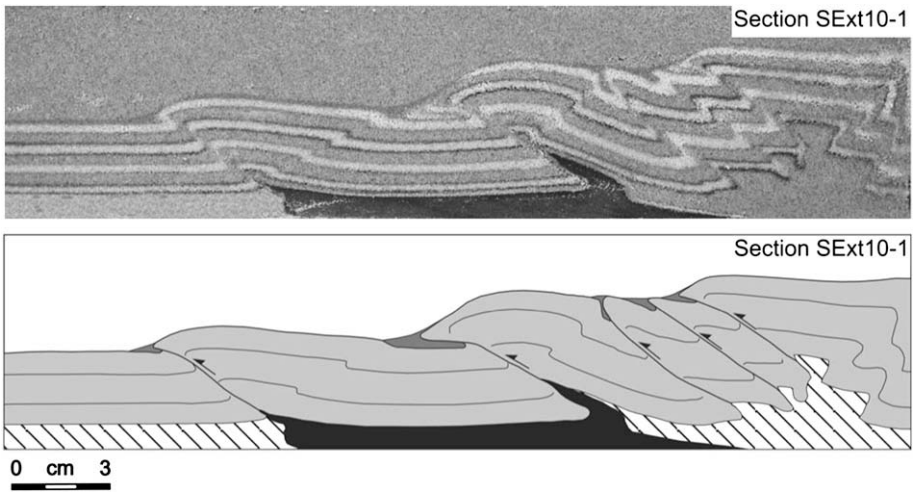

Fig. 16. Pictures and line-drawings of a parallel-to-shortening section of model SExt10 (see Fig. 15 for location) showing the low friction domain. Black area represents the ductile layer (SGM-36). In this case, the structural style is characterised by predominant foreland-verging thrusts with associated small backward structures developed in the back limbs.

explanation for this rotation and complement the knowledge of the structural evolution of CES with new insights about how to generate oblique and perpendicular structures. According to the paleomagnetic data, a clockwise rotation of up to 40° took place in the Pico del Águila anticline. In fact, the rotation documented in the field is also visible in the models presented in this study (Fig. 18) and we argue that no additional mechanism is needed to accommodate the rotation. In the models, at the boundary zones between the ductile and frictional décollements, the passive grid markers (placed at the surface of he models before shortening) locally show a rotation of up to *ca.* 30° from their initial position during the differential propagation of the deformation front. In other words, the rotation in the overburden units is a direct response to the differential propagation; further propagation of the deformation front above the ductile décollement and its retard above the high friction décollement lead to rotation of the markers/layers locally. Model results show that the rotation is bimodal (clockwise on one limb of the anticline and anti-clockwise on the other).

Until now, no viable explanation satisfying the relatively well-known geology of the area and the field observations has been proposed to explain the formation of these structures at such a high angle. In this contribution, we are demonstrating that it is possible to generate structures at high angle and even perpendicular to shortening direction with a single event of shortening. It is argued here that generation of the N–S trending structures of CES is likely to be the result of differential propagation of the deformation front above mechanical contrasts in the basal décollement (generation of structures at very high angle). With progressive shortening, this differential propagation also must have lead to rotation of the high-angle-trending structures at the boundary areas between the low and high friction décollements.

Based on field evidences about the distribution of the Triassic detachment, models were prepared to study the effect of changes in the mechanical behaviour of basal detachment on the generation of these oblique and transverse structures. In addition, the main outcropping rocks in the core of N–S trending structures are competent Upper Muschelkalk limestones and dolomites (M3 facies; Middle Triassic). Consequently, it is interpreted here that transverse anticlines are less likely to have been detached on less competent Upper Triassic rocks. The combination of these factors led us to think about a different distribution of deformation due to

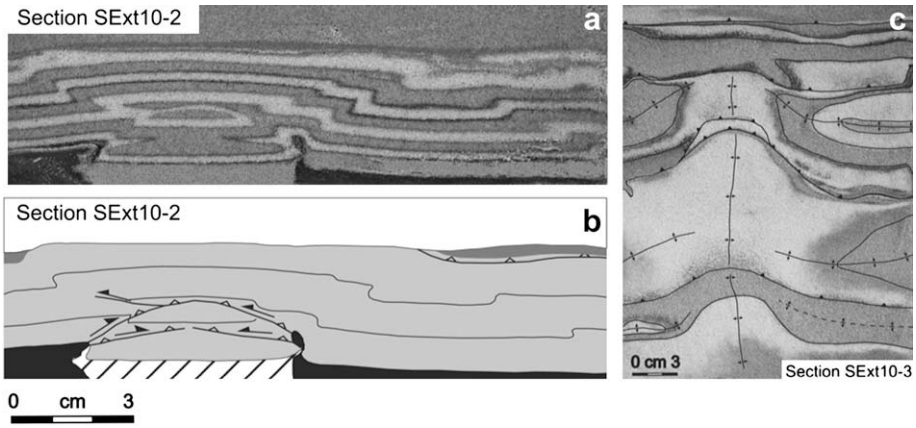

Fig. 17. Pictures and line-drawings of perpendicular-to-shortening and horizontal sections of model SExt10 (see Fig. 15 for location). Section SExt10-2 clearly shows the additional uplift of HF areas with regard to LF areas. In addition, deformation is assimilated by high faulting in the lower units and by gentle folding and small oblique reverse faults in the upper units (the small faults caused for the pure brittle behaviour of loose dry sand). Notice the thickening of ductile layers towards HF areas, and how lateral ramps detach on LF/HF limits and merge in the core of the structure, uplifting the upper units. Section SExt10-3 shows the interference structural pattern between orogen-parallel and transverse structures. This provides valuable information since allows to observe how units modify their geometry when changing the behaviour of the basal décollement.

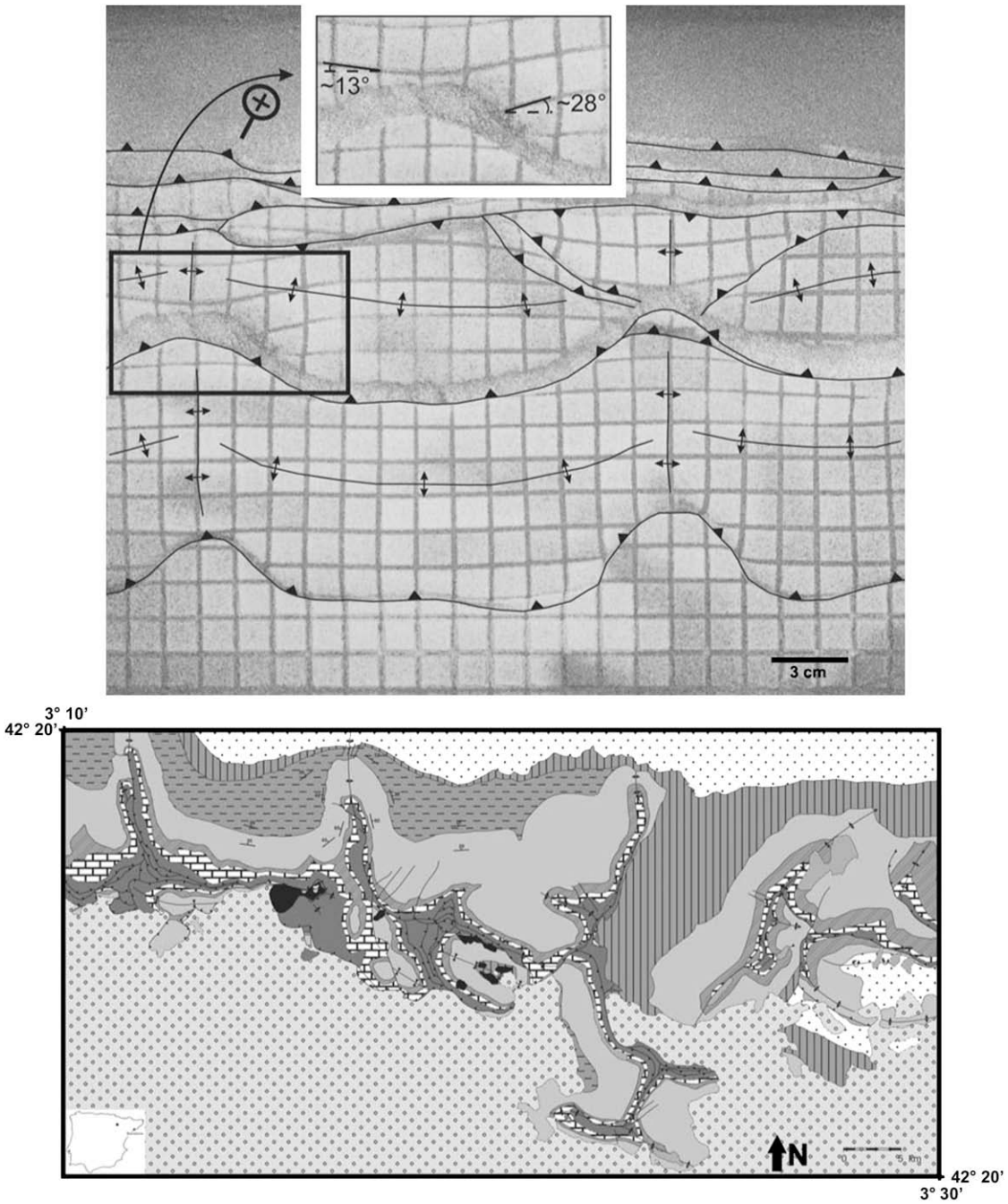

Fig. 18. Comparison between the last stage of model SExt10 in top view and the geological map of Central External Sierras (modified from IGME, 1992). Notice the geometrical similarities between both pictures: larger advance of areas performing orogen-parallel structures (LF areas in the model), and generation of transverse N–S anticlines, internally thrusted (HF areas in the model). The enlarged view shows the vertical axis rotation of the grid markers in the HF areas.

an uneven distribution of the basal detachment level in this part of the External Sierras.

After exploring two different parameters systematically, models have reproduced the general structural style of the area. Geometrical similarities between the mapped structures and models can be observed at regional scale in Fig. 18 and at single-structure scale in Fig. 19. Model results show that formation of oblique and orogen-perpendicular structures depends on the cover/detachment thickness ratio and the width of high friction detachment areas between the ductile décollements. Since the sedimentary cover is partially detached on a frictional material and partially detached on a ductile material, forming arcuate, oblique and transverse structures is only a matter of differential advance of the deformation front, which depends on the initial geometry and distribution of the ductile detachment.

In model Series A, we tested the thickness ratio between cover and detachment as a possible factor controlling the generation of orogen-perpendicular structures. For a given constant width of the HF areas (i.e. the distance between the ductile layers; 3 cm in Series A models), the different behaviour of the experiments depends on the sand cover thickness. This led us to consider the thickness ratio between cover and décollement layers as a parameter controlling the generation of oblique/transverse structures. In other words, there is a minimum value of cover thickness from which HF areas

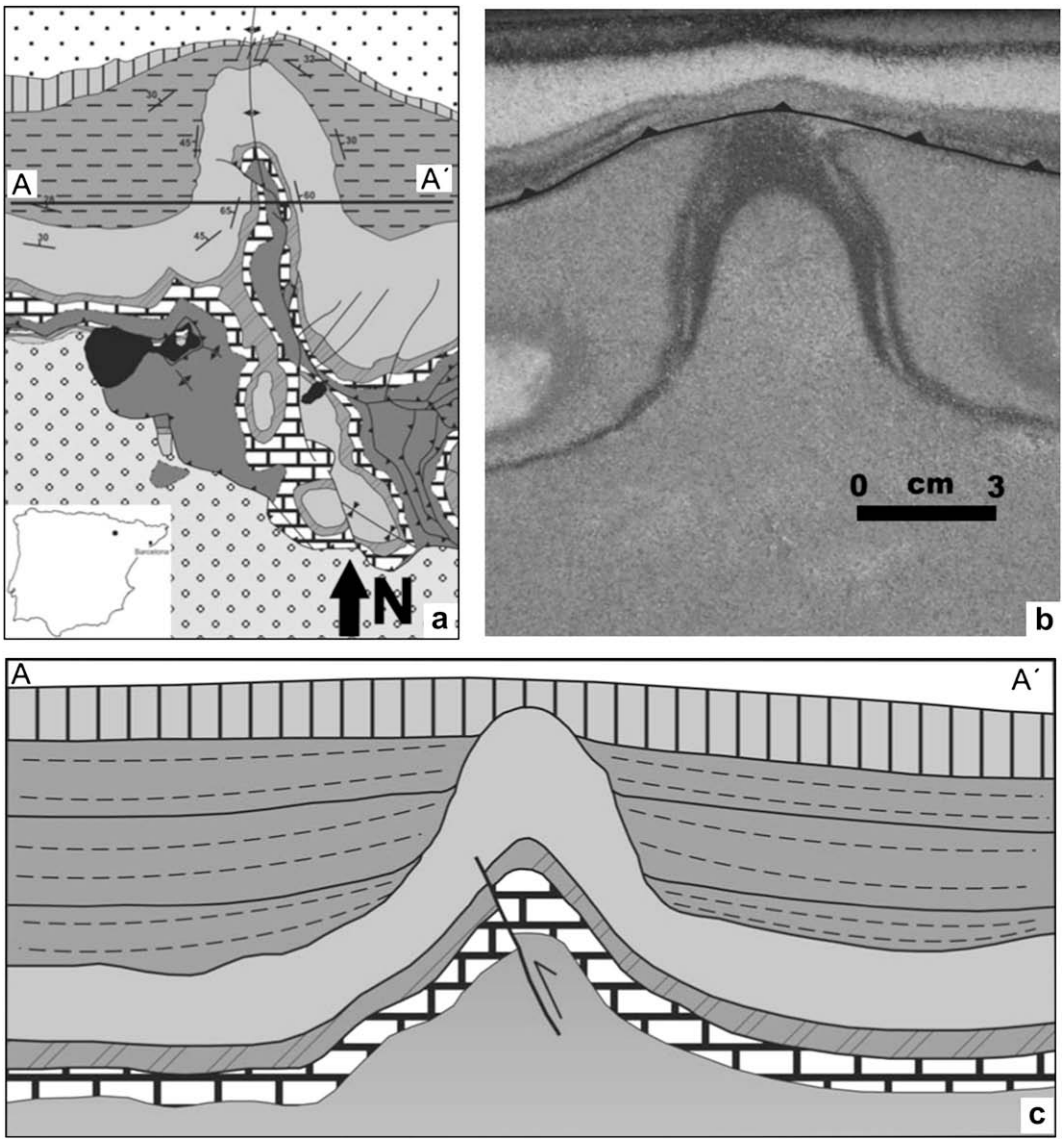

Fig. 19. Comparison between Pico del Águila geological map (modified from IGME, 1992) (a), a detailed horizontal section taken from the model (b), and a schematic cross-section generated from the 3D reconstruction of the Pico del Águila anticline (c; see Fig. 4). In (a) and (b) shortening comes from the top of the picture (~transport direction towards the south). Despite the geometrical similarities, notice that in (a) the thickness decrease of the units adjacent to the anticline is due to a thinning of the syntectonic growth strata towards the crest, whereas in (b) there is no thickness decrease but the emplacement of a thrust affecting the entire sequence (in this work no syntectonic sedimentation was added at any model during shortening).

become too narrow to affect the geometry of the structures while they advance. Decreasing the ratio of cover/décollement layer thicknesses results in formation of oblique structures, which may become transverse as cover thickness decreases further.

Since we are focusing on the most external unit of the orogen (South-Pyrenean thrust front at the southern limit of the Jaca Eocene piggy-back basin), the pre-kinematic stratigraphic sequence of the area is one of the thinnest (around 1100 m in Pico del Águila area) with regard to other Pyrenean structural units. In this area, only a thin sequence of Triassic units is preserved (outcropping around 300 m thick), and neither Jurassic nor Lower Cretaceous units are present. A thin sequence of Santonian–Maastrichtian rocks (around 150 m thick) is found in the area. Above this, units of the Cretaceous/Tertiary transition (Garumnian facies) are *ca.* 100 m thick, covered by 475–1000 m of Lutetian limestones (Guara Fm) that thin westward (Millán, 1995). In total, the pre-kinematic cover sequence ranges between 750 and 1250 m, whereas the Triassic detachment is considered to be approximately 300 m thick. Consequently, the thickness ratio between cover and detachment ranges from 2.5 (Eastern Central External Sierras) to 4.1 (Western Central External Sierras). In the models, the ratios considered have been 1.86 for SExt6, 3.83 for SExt9, 4.71 for SExt8 and 2.75 for SExt10. As mentioned earlier, oblique and transverse structures have formed only in models SExt6 and SExt10 where the thickness ratio is below the range observed in the field. For ratio values above 4.1 (SExt8) a homogeneous orogen-parallel structural pattern is observed and no clear oblique-transverse structures have been obtained. For ratios close to the upper limit (SExt9), the structural style changes between HF and LF areas but only slight wavy structures have been obtained (Figs. 7b and 9).

Width of the HF area between two ductile layers has also a significant influence on the formation of oblique and orogen-perpendicular structures. This is clearly shown when comparing top views of models SExt6 and SExt10 after 20% of shortening (Figs. 7a and 15). Due to the larger cover thickness in model SExt10, structures are bigger than in model SExt6. In nature, transverse anticlines of Central

External Sierras become shorter towards the West (Puigdefàbregas, 1975; Millán et al., 1994; Millán, 1995), and thickness of Guara Fm. ranges from 1000 m in Nasarre and Balces anticlines (Eastern Central External Sierras) down to 475 m in Bentué de Rasal and Pico del Águila anticlines (Western Central External Sierras). The combination of these facts led us to consider that the decrease in size of these anticlines towards the west is a consequence of the thickness decrease of Guara Fm. In such a way, cover thickness influences not only the formation but also the size of the oblique and transverse structures. In addition, the decrease of thickness of the cover influences in the relative strength between the brittle and the ductile layer, conditioning the geometry and size of the structures (Smit et al., 2003).

Model results show that there is a minimum HF width for a given cover thickness beyond which oblique and transverse structures do not form. Below this value, HF areas become too narrow and orogen-parallel thrusts advance forward regardless of the mechanical contrast in the basal level. For wider HF areas, the geometry of the structures becomes gentler and more open and their wavelength increases. In such a way, narrow HF areas produce tighter folds. This observation from the models is important to understand the different geometry between the orogen-perpendicular anticlines of Central External Sierras. Pico del Águila anticline in the west is a tight, nearly isoclinal fold (Millán, 1995) whereas Gabardiella anticline complex shows a gentler, more open geometry, with a larger wavelength (Fig. 1). In such a way, the superficial geometry of the folds can provide an idea about the approximate distribution of the detachment level in depth and/or the thickness ratio between the cover and ductile units.

Both studied parameters (i.e. cover/detachment thickness ratio and width of HF areas) can be considered together by plotting them in a unique graph (Fig. 20). If we divide the thickness ratio (parameter A) by the width of HF areas (parameter B), we obtain the ratio *k*. This new parameter gives an idea of the suitable proportions within which oblique and transverse structures may develop. According to model results, orogen-oblique and orogen-transverse structures may form for $k < 1$ (models SExt6 and SExt10), whereas for $k > 1$ only orogen-parallel structures are obtained (models SExt8 and SExt9) (Table 2). Therefore, oblique and transverse structures may develop if the width of the HF areas is larger than a well-suited ratio between cover and décollement thicknesses.

Transverse and oblique anticlines of Central External Sierras display the highest structural relief of the area, reaching the highest topographic altitudes and creating the main mountain chains in the region. Model results reproduced this behaviour above the HF areas where a significant amount of uplift takes place relative to the LF areas (Figs. 14 and 17a,b).

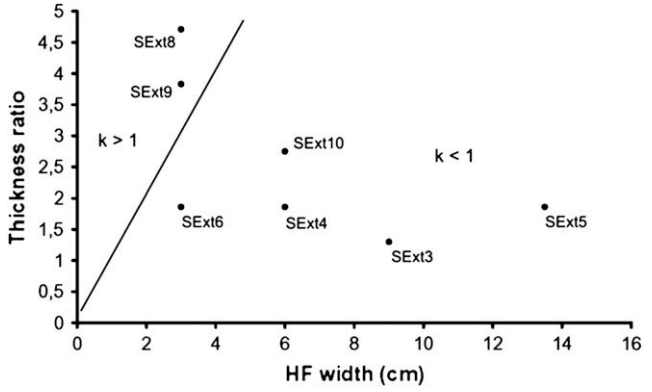

Fig. 20. Plot of the cover/detachment thickness ratio against width of HF areas. The parameter k indicates the ratio between thickness ratio and HF width. Oblique and transverse structures may form if HF width is larger than the thickness ratio ($k < 1$).

Table 2
Cover/décollement thickness ratio, width of HF areas and *k* value of each model.

Model	Thickness ratio	HF width	*k* value[a]	Transverse structures obtained?
SExt6	1.86	3	0.62	Yes
SExt8	4.71	3	1.57	No
SExt9	3.83	3	1.1	No
SExt10	2.75	6	0.46	Yes
SExt3[b]	1.3	9	0.14	Yes
SExt4[b]	1.86	6	0.31	Yes
SExt5[b]	1.86	13.5	0.14	Yes

[a] *k* is equal to the thickness ratio divided by the width of the HF areas.
[b] Models SExt3, SExt4 and SExt5 were also performed in the same series of experiments, although not discussed in this study.

The use of loose sand and silicone in analogue modelling presents some limitations when reproducing certain case-studies (for a detailed description of materials, properties and their suitability as analogues see Weijermars, 1986; and Weijermars and Schmeling, 1986). As stated, models have reproduced the differential uplift of HF areas by means of gentle anticlines in the upper units, usually showing open limbs uplifted by two lateral ramps that merge in the core of the structure. In other cases, this extra uplift of the upper units is solved via some local oblique small-throw reverse faults. However, transverse anticlines of Central External Sierras perform steep dipping, in some cases overturned limbs, and a higher plunge value towards the hinterland. Due to the mechanical behaviour of loose cohesionless sand, it becomes easily faulted when a minimum amount of deformation is applied. Consequently, it is not possible to reproduce such geometry observed in nature by using loose sand to model the entire sedimentary cover. The stratigraphy of the area is more complex in terms of mechanical behaviour, exhibiting an interlayering of brittle-plastic materials that allow the generation of steep dipping folds. Despite this, if a sand–silicone multilayering was used to model the sedimentary cover, and syn-kinematic sedimentation was added, higher dip values of a gravitationally stable pre-kinematic sequence could be achieved (Nalpas et al., 1999, 2003). In this sense, improving the mechanical stratigraphy by using multiple décollements as secondary detachment levels (Nalpas et al., 1999; Massoli et al., 2006) would help in the construction of higher steeper structures.

6. Conclusions

Model results provide new insights on the evolution of the oblique and transverse structures of the Central External Sierras. Based on the uneven distribution of the Triassic detachment level, models simulate the characteristics of the N–S trending anticlines of Central External Sierras: generation synchronous with the emplacement of the South-Pyrenean frontal thrust, higher structural relief compared to orogen-parallel structures, absence of a representative ductile décollement in the core, faulting of lower units and folding of upper ones, plunge towards the hinterland, and foreland-side closure not thrusted by the frontal emerging South-Pyrenean thrust. The generation of the N–S structures of CES (at high angle to the shortening direction) and the rotation documented in the field are illustrated to be due to differential propagation of the deformation front above mechanical contrasts in the basal décollement.

Acknowledgements

We would like to thank Alejandro Amilibia and Ruth Soto for their brilliant ideas and suggestions. Paradigm™ is acknowledged

for providing a GoCad® Academic license. Authors also wish to thank the Group of Geodynamics and Basin Analysis (GGAC) at Universitat de Barcelona. This research has been supported by StatoilHydro, the Geomod 3D project (CGL2004-05816-C02-01/BTE), the MODES-4D project (CGL2007-66431-C02-01/BTE) and the Geomodels Institute Consortium. O. Vidal-Royo wish to thank Agència de Gestió d'Ajuts Universitaris i a la Recerca (AGAUR) for providing a PhD grant (2005 FI 00200) and additional funds (2006 BE-2 00095) for a 3-month stay at Hans Ramberg Tectonic Laboratory of Uppsala University. H.A. Koyi is funded by the Swedish Research Council (VR). Authors are grateful to Dr. M. Bonini for a thorough and constructive review, which improved both the content and presentation of the manuscript. An anonymous reviewer is also acknowledged for comments and suggestions.

References

Almela, A., Ríos, J.M., 1951. Mapa geológico de España 1:50000 serie Antigua, 248 (Apiés). IGME Ed.Madrid, 50 pp + map.

Anastasio, D.J., 1992. Structural evolution of the External Sierras, Southern Pyrenees, Spain. In: Mitra, S., Fisher, G.W. (Eds.), Structural Geology of Fold and Thrust Belts. Johns Hopkins University Press, Baltimore, pp. 239–251.

Anastasio, D.J., Holl, J.E., 2001. Transverse fold evolution in the External Sierras, Southern Pyrenees, Spain. Journal of Structural Geology 23 (2–3), 379–392.

Bahroudi, A., Koyi, H.A., 2003. Effect of spatial distribution of Hormuz salt on deformation style in the Zagros fold and thrust belt: an analogue modeling approach. Journal of the Geological Society 160, 719–733.

Beaumont, C., Muñoz, J.A., Hamilton, J., Fullsack, P., 2000. Factors controlling the Alpine evolution of the central Pyrenees inferred from a comparison of observations and geodynamical models. Journal of Geophysical Research 105, 8121–8145.

Bentham, P., Burbank, D.W., 1996. Chronology of Eocene foreland basin evolution along the western oblique margin of the South-Central Pyrenees. In: Friend, P.F., Dabrio, C.J. (Eds.), Tertiary Basins of Spain. Cambridge University Press, Cambridge, pp. 144–152.

Bonini, M., 2003. Detachment folding, fold amplification, and diapirism in thrust wedge experiments, Tectonics, 22(6), 1065, doi:10.1029/2002TC001458.

Bonini, M., 2007. Deformation patterns and structural vergence in brittle-ductile thrust wedges: an additional analogue modelling perspective. Journal of Structural Geology 29, 141–158.

Castillo-Herrador, F., 1974. Le Trias évaporitique des basins de la Vallée de l'Ebre et de Cuenca. Bulletin de la Societé Géologique de France 16, 49–63.

Cobbold, P.R., Rossello, E.A., Vendeville, B.C., 1989. Some experiments on interacting sedimentation and deformation above salt horizons. Bulletin de la Societé Géologique de France 8, 453–460.

Costa, E., Vendeville, B.C., 2002. Experimental insights on the geometry and kinematics of fold-and-thrust belt above weak, viscous evaporitic décollement. Journal of Structural Geology 24, 1729–1739.

Cotton, J.T., Koyi, H.A., 2000. Modelling of thrust fronts above ductile and frictional detachments: application to structures in the Salt Range and Potwar Plateau, Pakistan. Geological Society of America Bulletin 112, 351–363.

Crespo-Blanc, A., 2008. Recess drawn by the internal zone outer boundary and oblique structures in the paleomargin-derived units (Subbetic Domain, central Betics): an analogue modeling approach. Journal of Structural Geology 30, 65–80.

Davis, D.M., Engelder, T., 1985. The role of salt in fold-and-thrust belts. Tectonophysics 119, 67–88.

Dinarés, J., McClelland, E., Santanach, P., 1992. Contrasting rotations within thrust sheets and kinematics of thrust tectonics as derived from paleomagnetic data: an example from the Southern Pyrenees. In: McClay, K.R. (Ed.), Thrust Tectonics. Chapman & Hall, London, pp. 265–276.

Dooley, T.P., Jackson, M.P.A., Hudec, M.R., 2007. Initiation and growth of salt-based thrust belts on passive margins: results from physical models. Basin Research 19, 165–177.

Grelaud, S., Nalpas, T., Vergés, J., Karpuz, R., 2002. Role of décollement levels in thrust systems: field examples and analogue modelling. Bolletino di Geofisica teorica ed applicata, 42 N(½ Suppl.), 178–180.

Harrison, J.C., 1995. Tectonics and Kinematics of a foreland folded belt influenced by salt, Arctic Canada. In: Jackson, M.P.A., Roberts, D.G., Snelson, S. (Eds.), Salt Tectonics: A Global Perspective, vol. 65. AAPG Memoirs, pp. 379–412.

Hogan, P.J., Burbank, D.W., 1996. Evolution of the Jaca Piggyback basin and emergence of External Sierras, Southern Pyrenees. In: Friend, P.F., Dabrio, C.J. (Eds.), Tertiary Basins of Spain. Cambridge University Press, pp. 153–160.

Holl, J.E., Anastasio, D.J., 1993. Paleomagnetically derived folding rates, southern Pyrenees, Spain. Geology 21 (3), 271–274.

IGME, 1992. Mapa Geológico de España; Hoja 248, Apiés; Instituto Geológico y Minero de España, Madrid, Unpublished 36 pp report +1:50000 map.

Jurado, M.J., 1990. El Triásico y el Liásico basal evaporíticos del subsuelo de la cuenca del Ebro. In: Ortí, F., Salvany, J.M. (Eds.), Formaciones evaporíticas de la Cuenca del Ebro y cadenas periféricas, y de la zona de Levante. Enresa, Madrid, pp. 21–28.

Koyi, H.A., 1988. Experimental modeling of role of gravity and lateral shortening in Zagros mountain belt. AAPG Bulletin 72, 1381–1394.

Koyi, H.A., 1995. Mode of internal deformation in sand wedges. Journal of Structural Geology 17, 293–300.

Koyi, H.A., 1997. Analogue modelling: from a qualitative to a quantitative technique – a historical perspective. Journal of Petroleum Geology 20, 223–238.

Koyi, H.A., Vendeville, C.B., 2003. The effect of décollement dip on geometry and kinematics of model accretionary wedges. Journal of Structural Geology 25, 1445–1450.

Koyi, H.A., Cotton, J., 2004. Experimental insights on the geometry and kinematics of fold-and-thrust belts above weak, viscous evaporitic décollement; a discussion. Journal of Structural Geology 26, 2139–2141.

Koyi, H.A., Sans, M., 2006. Deformation transfer in viscous detachments: comparison of sandbox models to the South Pyrenean Triangle Zone. Geological Society, London, Special Publications, January 1, 2006; vol. 253(1), pp. 117-134.

Larrasoaña, J.C., Parés, J.M., Pueyo, E.L., 2001. Stable eocene magnetization carried by magnetite and iron sulphides in marine marls (Pamplona-Arguis Formation, Southern Pyrenees, Northern Spain). Studia Geophysica et Geodaetica 47 (2), 237–254.

Letouzey, J., Colletta, B., Vially, R., Chermette, J.C., 1995. Evolution of salt-related structures in compressional settings. In: Jackson, M.P.A., Roberts, D.G., Snelson, S. (Eds.), Salt Tectonics: A Global Perspective, vol. 65. American Association of Petroleum Geologists Memoir, pp. 41–60.

Liu, H., McClay, K.R., Powell, D., 1992. Physical models of thrust wedges. In: McClay, K.R. (Ed.), Thrust Tectonics. Chapman & Hall, pp. 71–81.

Lohrmann, J., Kukowski, N., Adam, J., Oncken, O., 2003. The impact of analogue material properties on the geometry, kinematics and dynamics of convergent sand wedges. Journal of Structural Geology 25, 1691–1711.

López-Gómez, K., Arche, A., Pérez-López, A., 2002. Permian and Triassic. In: Gibbons, W., Moreno, T. (Eds.), The Geology of Spain. The Geological Society of London, pp. 185–212.

Luján, M., Storti, F., Balanyá, J.C., Crespo-Blanc, A., Rosetti, F., 2003. Role of décollement material with different rheological properties in the structure of the Aljibe thrust imbricate (Flysch Trough, Gibraltar Arc): an analogue modelling approach. Journal of Structural Geology 25, 867–881.

Mallada, L., 1878. Geología de la provincial de Huesca. Mem. Com. Mapa geológico de España, Madrid, 559 pp.

Marques, F.O., Cobbold, P.R., 2002. Topography as a major factor in the development of arcuate thrust belts: insights from sandbox experiments. Tectonophysics 348, 247–268.

Marques, F.O., Cobbold, P.R., 2006. Effects of topography on the curvature of fold-and-thrust belts during shortening of a 2-layer model of continental lithosphere. Tectonophysics 415, 65–80.

Massoli, D., Koyi, H.A., Barchi, M.R., 2006. Structural evolution of a fold and thrust belt generated by multiple décollements: analogue models and natural examples from Northern Apennines (Italy). Journal of Structural Geology 28, 185–199.

McClay, K.R., Whitehouse, P., 2004. Analogue modelling of doubly vergent thrust wedges. In: McClay, K.R. (Ed.), Thrust Tectonics and Hydrocarbon Systems, vol. 82. American Association of Petroleum Geologists, Memoir, pp. 372–399.

McClay, K.R., Whitehouse, P.S., Dooley, T., Richards, M., 2004. 3D evolution of fold and thrust belts formed by oblique convergence. Marine and Petroleum Geology 21, 857–877.

Millán, H., 1995. Estructura y Cinemática del frente de cabalgamiento surpirenaico en las Sierras Exteriores Aragonesas; PhD Thesis, Departamento de Ciencias de la Tierra, Universidad de Zaragoza, Zaragoza, 330 pp + annex.

Millán, H., Aurell, M., Meléndez, A., 1994. Synchronous detachment folds and coeval sedimentation in the Prepyrenean External Sierras (Spain): a case study for a tectonic origin of sequences and system tracts. Sedimentology 41 (5), 1001–1024.

Mulugeta, G., 1988. Modelling the geometry of Coulomb thrust wedges. Journal of Structural Geology 10, 847–859.

Mulugeta, G., Koyi, H.A., 1987. Three-dimensional geometry and kinematics of experimental piggy-back thrusting. Geology 15, 1052–1056.

Mulugeta, G., Koyi, H., 1992. Episodic accretion and strain partitioning in a model sand wedge. Tectonophysics 202, 319–333.

Muñoz, J.A., 1992. Evolution of a continental collision belt: ECORS-Pyrenees crustal balanced cross-section. In: McClay, K.R. (Ed.), Thrust Tectonics. Chapman & Hall, pp. 235–246.

Nalpas, T., Györfi, I., Guillocheau, F., Lafont, F., Homewood, P., 1999. Influence de la charge sédimentaire sur le développement d'anticlinaux synsédimentaires. Modélisation analogique et exemple du terrain (bordure sud du basin de Jaca). Bulletin de la Societé Géologique de France 170 (5), 733–740.

Nalpas, T., Gapais, D., Vergés, J., Barrier, L., Gestain, V., Leroux, G., Rouby, D., Kermarrec, J.J., 2003. Effects of rate and nature of synkinematic sedimentation on the growth of compressive structures constrained by analogue models and field examples. In: McCant, T., Saintot, A. (Eds.), Tracing Tectonic Deformation Using the Sedimentary Record, vol. 208. Geological Society, London, Special Publications, pp. 307–319.

Nilforoushan, F., Koyi, H.A., Swantesson, J.O.H., Talbot, C.J., 2008. Effect of basal friction on surface and volumetric strain in models of convergent settings measured by laser scanner. Journal of Structural Geology 30, 366–379.

Oliva, B., Millán, H., Pocoví, A., Casas, A.M., 1996. Estructura de la Cuenca de Jaca en el sector occidental de las Sierras Exteriores Aragonesas. Geogaceta 20 (4), 800–802.

Oliva-Urcía, B., Pueyo, E.L., 2007. Gradient of shortening and vertical-axis rotations in the Southern Pyrenees (Spain), insights from a synthesis of paleomagnetic data. Revista de la Sociedad Geológica de España 20 (1–2), 105–118.
Poblet, J., Hardy, S., 1995. Reverse modeling of detachment folds; application to the Pico de Aguila anticline in the south central Pyrenees (Spain). Journal of Structural Geology 17 (12), 1707–1724.
Poblet, J., McClay, K.R., Storti, F., Muñoz, J.A., 1997. Geometries of syntectonic sediments associated with single-layer detachment folds. Journal of Structural Geology 19 (3–4), 369–381.
Pocoví, A.J., 1979. Estudio geológico de las Sierras Marginales Catalanas (Prepirineo de Lérida). Acta Geológica Hispánica 13, 73–79.
Pueyo, E.L., 2000. Rotaciones Paleomagnéticas en Sistemas de Pliegues y Cabalgamientos. Tipos, Causas, Significado y Aplicaciones (Ejemplos de las Sierras Exteriores y Cuenca de Jaca, Pirineo Aragonés); PhD Thesis, Departamento de Ciencias de la Tierra, Universidad de Zaragoza, Zaragoza, 300 pp + annex.
Pueyo, E.L., Millán, H., Pocoví, A., Parés, J.M., 1997. Determination of the folding mechanism by AMS data: study of the relation between shortening and magnetic anisotropy in the Pico del Águila anticline (Southern Pyrenees). Physics and Chemistry of the Earth 22 (1–2), 195–201.
Pueyo, E.L., Millán, H., Pocoví, A., Parés, J.M., 2000. Cinemática rotacional del cabalgamiento basal surpirenaico en as Sierras Exteriores Aragonesas: datos magnetotectónicos. Acta Geológica Hispánica 32 (3–4), 119–137.
Pueyo, E.L., Millán, H., Pocoví, A., 2002. Rotation velocity of a thrust: a paleomagnetic study in the External Sierras (Southern Pyrenees). Sedimentary Geology 146 (1), 191–208.
Pueyo, E.L., Pocoví, A., Parés, J.M., Millán, H., Larrasoaña, J.C., 2003a. Thrust ramp geometry and spurious rotations of paleomagnetic vectors. Studia Geophysica Geodetica 47, 331–357.
Pueyo, E.L., Parés, J.M., Millán, H., Pocoví, A., 2003b. Conical folds and apparent rotations in paleomagnetism (a case study in the Southern Pyrenees). Tectonophysics 362, 345–366.
Puigdefàbregas, C., 1975. La Sedimentación Molásica en la Cuenca de Jaca; Monografias del Instituto de Estudios Pirenaicos. Número Extraordinario de Revista Pirineos, 104, Instituto de Estudios Pirrenaicos, Jaca, 153 pp + annexes.
Salvany, J.M., 1990. Introducción a las evaporitas triásicas de las cadenas periféricas de la cuenca del Ebro: Catalánides, Pirineo y Región Cantábrica. In: Ortí, F., Salvany, J.M. (Eds.), Formaciones evaporíticas de la Cuenca del Ebro y cadenas periféricas, y de la zona de Levante. Enresa, Madrid, pp. 21–28.
Schreurs, G., Hänni, R., Vock, P., 2002. Analogue modeling of transfer zones in fold and thrust belts: a 4-D analysis. Journal of the Virtual Explorer 6, 43–49.
Selzer, G., 1948. Geología de las sierras surpirenaicas del Alto Aragón. (Translated from the original version, "Geologie der sudpyrenäische Sierren inOberaragonien", Berlin, 1934). Publicación Extraordinaria Geol. España. C.S.I.C.; Madrid, IV, pp. 185–231.
Smit, J.H.W., Brun, J.P., Sokoutis, D., 2003. Deformation of brittle-ductile thrust wedges in experiments and nature. Journal of Geophysical Research 108 (B10), 2480, doi:10.1029/2002JB002190.
Soler, M., Puigdefàbregas, C., 1970. Líneas generales de la geología del Alto Aragón Occidental. Pirineos 96, 5–20.
Soto, R., Casas, A.M., Storti, F., Faccena, C., 2002. Role of lateral thickness variations on the development of oblique structures at the Western end of the South Pyrenean Central Unit. Tectonophysics 350, 215–235.
Soto, R., Casas-Sainz, A.M., Pueyo, E.L., 2006. Along-strike variation of orogenic wedges associated with vertical axis rotations. Journal of Geophysical Research 111, B10402, doi:10.1029/2005JB004201.
Storti, F., Soto-Marin, R., Faccena, C., Casas-Sainz, A., 2001. Role of the backstop-to-cover thickness ratio on vergence partitioning in experimental thrust wedges. Terra Nova 13 (6), 413–417.
Storti, F., Soto-Marin, R., Rossetti, F., Casas-Sainz, A., 2007. Evolution of experimental thrust wedges accreted from along-strike tapered, silicone-floored multilayers. Journal of the Geological Society of London 164, 73–85.
Swantesson, J.O.H., 2005. Weathering and erosion of rock carvings in Sweden during the period 1994–2003. Micro Mapping with Laser Scanner for Assessment of Breakdown Rates, 29. Karlstad University Studies, pp. 99.
Swantesson, J.O.H., Moses, C.A., Berg, G.E., Jansson, M.J., 2006. Methods for measuring shore platform micro erosion: a comparison of the micro-erosion meter and laser scanner. Zeitschrift für Geomorphologie N.F 144 (Suppl), 1–17.
Talbot, C.J., 1992. Centrifuge models of Gulf of Mexico profiles. Marine and Petroleum Geology 9, 412–432.
Teixell, A., García-Sansegundo, J., 1995. Estructura del sector central de la Cuenca de Jaca (Pirineos Meridionales). Revista de la Sociedad Geológica de España 8 (3), 215–228.
Teixell, A., Koyi, H.A., 2003. Experimental and field study of the effects of lithological contrasts on thrust-related deformation. Tectonics 22, 1054, doi:10.1029/2002TC001407.
Weijermars, R., 1986. Flow behaviour and physical chemistry of bouncing putties and related polymers in view of tectonic laboratory applications. Tectonophysics 124, 325–358.
Weijermars, R., Schmeling, H., 1986. Scaling of Newtonian and non-Newtonian fluid dynamics without inertia for quantitative modelling of rock flow due to gravity (including the concept of rheological similarity). Physics of the Earth and Planetary Interiors 43, 316–330.
Williams, R.B.G., Swantesson, J.O.H., Robinson, D.A., 2000. Measuring rates of surface downwearing and mapping microtopography: the use of micro-erosion meters and laser scanners in rock weathering studies. Zeitschrift für Geomorphologie N.F 120 (Suppl), 51–66.